https://doi.org/10.5194/egusphere-2026-6632
Preprint. Discussion started: 19 November 2026
© Author(s) 2026. CC BY 4.0 License.

Black and brown carbon deposited onto boreal snow: Distinct optical evolution and redistribution during melt

Delun Li[1], Krista Luoma[1], Jonas Svensson[1], Meri M. Ruppel[1,2], Ilpo Marja-Aho[1], Hans Moosmüller[3], Aki Virkkula[1]

[1]Atmospheric composition research unit, Finnish Meteorological Institute, Helsinki, Finland
[2]Department of Environmental Sciences, University of Helsinki, Helsinki, Finland
[3]Division of Atmospheric Sciences, Desert Research Institute, Reno, NV, USA

Correspondence to: Delun Li (delun.li@fmi.fi)

Abstract. Light-absorbing black and brown carbon (BC and BrC, respectively) deposited onto snow enhance solar absorption. However, their optical properties and vertical distribution may change as snow ages and is exposed to ambient weather. These processes remain poorly understood. To quantify their temporal evolution, birch- and peat-combustion emissions were deposited onto natural snow in a controlled field experiment in subarctic Finland. The optical properties of water-soluble BrC (WS-BrC), methanol-soluble BrC (MS-BrC), and BC were followed for up to five weeks until snow meltout. At the snow surface, the WS-BrC absorption Ångström exponent (AAE) at 370–470 nm decreased from approximately 9 to 6 within two weeks for both fuels, whereas MS-BrC AAE changes differed between fuels. Mass absorption cross-section (MAC) at 370 nm decreased from 2.0 to 1.2 $m^2\ g^{-1}$ for birch-derived MS-BrC and from 0.4 to 0.1 $m^2\ g^{-1}$ for peat-derived MS-BrC. BC MAC decreased from 17.8 to 4.5 $m^2\ g^{-1}$ over three weeks. The changes in BrC optical properties are consistent with photobleaching. As snow metamorphism progressed, WS-BrC was redistributed deeper into the snowpack, whereas MS-BrC and BC remained mainly near the surface, with some downward redistribution when reaching near-isothermal conditions. These observations demonstrate that post-depositional changes in the optical properties and vertical distribution of BrC and BC may influence the magnitude and distribution of solar absorption within snow, with potential implications for snowmelt and snow–albedo feedbacks.

1 Introduction

Incomplete combustion of biomass and fossil fuels emits greenhouse and trace gases and particulate matter (PM). The PM mass is typically dominated by light-absorbing black carbon (BC) and organic carbon (OC) particles, with emissions that depend strongly on fuel type and combustion phase. Globally, BC causes the strongest warming of all atmospheric particle types, with its direct atmospheric absorption causing a global radiative forcing of +0.71 W m^{-2} for the industrial era (1750–2005) (Bond et al., 2013). Deposition of BC onto snow and ice reduces surface albedo and thereby provides an additional positive forcing, assessed as +0.08 W m^{-2} in 2019 relative to 1750 (Forster et al., 2021). OC is a complex mixture of organic

https://doi.org/10.5194/egusphere-2026-6632
Preprint. Discussion started: 19 November 2026
© Author(s) 2026. CC BY 4.0 License.

compounds, including hydrocarbons and oxygen- and nitrogen-containing species, and therefore also its optical properties vary (Laskin et al., 2015; Li et al., 2020; Barreira et al., 2024). OC can be purely scattering, or it can absorb light especially on short wavelengths. In climate models, OC has been considered as primarily scattering, but more recent research has shown that a substantial fraction of OC strongly absorbs radiation at ultraviolet and visible wavelengths. This short-wavelength light-absorbing component of OC is commonly referred to as brown carbon (BrC) (Andreae and Gelencsér, 2006; Laskin et al., 2015).

When deposited onto snow, BC and BrC have a strong climate impact as they darken the snow surface and enhance solar energy absorption, thereby accelerating melt (Flanner et al., 2007; Zhu et al., 2024). This snow-darkening effect is particularly consequential in high-latitude and high-elevation regions, where strong snow-albedo feedbacks can amplify warming and accelerate snowmelt (Hansen et al., 2005; Flanner et al., 2007; Rantanen et al., 2022). While the radiative effects and optical properties of BC deposited onto snow have been widely investigated using both field observations and modelling (e.g., Flanner et al., 2007; Hadley and Kirchstetter, 2012; Wang et al., 2013; Doherty et al., 2014; He et al., 2018; Svensson et al., 2024), the radiative contribution of BrC deposited onto snow remains less constrained, with most data/observations coming from a small set of field studies in regions such as the Himalayas, North America, and the Arctic (e.g., Voisin et al., 2012; Zhang et al., 2019; Beres et al., 2020).

Across studies, BrC is characterised differently, using metrics that include chemical composition and, more commonly, optical properties. Because BrC absorption is strongly wavelength dependent, it is often described by a relatively high absorption Ångström exponent (AAE $\gg$ 1), whereas BC typically has an AAE close to 1 (Moosmüller et al., 2009). Related quantities such as mass absorption cross-section (MAC) and wavelength-resolved absorption are also frequently reported. Controlled laboratory ageing measurements and atmospheric observations commonly show net decreases in BrC aerosol absorptivity through photochemical bleaching (Forrister et al., 2015; Hems et al., 2021), whereas other reactions, such as nighttime chemical reactions, can produce compounds (e.g., nitroaromatics) that enhance absorption under certain conditions (Hems et al., 2021; Barreira et al., 2024). How these competing transformations proceed under changing snowpack conditions remains unclear, as radiation, temperature, and liquid water content greatly vary during melt. This uncertainty in how BrC ages likely contribute to the wide range of optical properties reported for BrC in snow. For example, AAE values range from ~1–6 for bulk or filtered snow samples and ~5–10 for solvent-isolated BrC fractions, while reported MAC values for BrC span ~0.45–4.7 $m^2\ g^{-1}$ (Doherty et al., 2010; Wang et al., 2013; Hu et al., 2018; Beres et al., 2020; Yan et al., 2020).

Post-depositional redistribution of light-absorbing carbon in snow is partly contrasting even for the better-known hydrophobic BC, with most studies suggesting strong near-surface retention and few others reporting substantial flushing during melt. Several studies have reported strong near-surface retention or enrichment during melt: Xu et al. (2009) observed increasing surface concentrations of BC and organic material on the Tibetan Plateau, and similar observation was found by Doherty et al.

https://doi.org/10.5194/egusphere-2026-6632
Preprint. Discussion started: 19 November 2026
© Author(s) 2026. CC BY 4.0 License.

(2013) in Alaska, Greenland and Norway. Sterle et al. (2013) and Chellman et al. (2026) reported retention or enrichment of BC and other insoluble light-absorbing particles near the snow surface in the Sierra Nevada of California, USA. In contrast, Lazarcik et al. (2017) documented rapid loss of a substantial fraction of BC from a melting snowpack in New Hampshire, USA. These contrasting observations indicate that post-depositional redistribution is strongly influenced by snowpack and melt conditions (Chellman et al., 2026) and can vary substantially between sites. BrC may behave differently because it contains both water-soluble and less soluble fractions, whereas BC is predominantly water insoluble. Water-soluble BrC (WS-BrC) may therefore be transported more readily with meltwater, while less soluble BrC may be retained or redistributed differently within the snowpack. Direct observations of BrC redistribution during snowmelt remain scarce, leaving considerable uncertainty in how its different fractions evolve and migrate during snow metamorphism and melt.

Here, we study these two linked processes that remain poorly constrained in snow: (i) the aging of BrC after deposition and (ii) the vertical redistribution of light-absorbing carbon particles during snow metamorphism and melt. To address these processes, we performed a unique controlled field deposition experiment, designed to follow BrC and BC optical evolution in natural snow over time and depth. BrC- and BC-containing emissions from peat and birch wood combustion were purposely deposited onto natural subarctic seasonal snow, after which the contaminated snow was repeatedly sampled during the melt season from the surface and at different depths within the snowpack over approximately five weeks. Our aims were to i) quantify temporal changes in AAE, MAC, and absorption for BrC and BC from atmospheric to newly snow surface deposited and aged particles, and to ii) evaluate how different light-absorbing carbon fractions were retained and redistributed as the snowpack metamorphoses and melts over about five weeks. We show that water- and methanol-soluble BrC (MS-BrC) and the mainly hydrophobic BC behave differently in the melting snowpack, and thus variably influence the light-absorption of surface snow, which has implications for snow radiative forcing.

2 Sampling and Methods

2.1 Sampling site and the SoS2023 campaign

The field experiment was conducted at an inactive Sodankylä airfield (67°23′ N, 26°36′ E) in northern Finland, near the Finnish Meteorological Institute (FMI) Sodankylä observatory in Tähtelä in March to May 2023. The site is located in a subarctic environment characterised by a long-lasting seasonal snow cover. The 1991–2020 annual mean temperature was 0.3 °C, the average snow depth in mid-March was ~75 cm, and the median snow cover period was from Sep 26 to May 14. FMI has previously performed several controlled field experiments (also known as soot-on-snow, SoS, experiments) at this site to study the effects of deposition of different particles, including light-absorbing carbon and mineral dust, onto natural snow affected by springtime weather conditions (Meinander et al., 2014; Peltoniemi et al., 2015; Svensson et al., 2024). The site is located within a secure, gated area, and the snow surface remained largely undisturbed during the observation period, which provided unique and suitable conditions to track how the deposited material evolved within the natural snowpack. In our 2023 SoS

https://doi.org/10.5194/egusphere-2026-6632
Preprint. Discussion started: 19 November 2026
© Author(s) 2026. CC BY 4.0 License.

experiment, aerosol particles were introduced into a chamber that was placed onto the snowpack and removed after 2 hours. Subsequently, albedo and snow properties were monitored through spring until snow meltout (Fig. 1), as previously described in Peltoniemi et al. (2015) and Svensson et al. (2024).

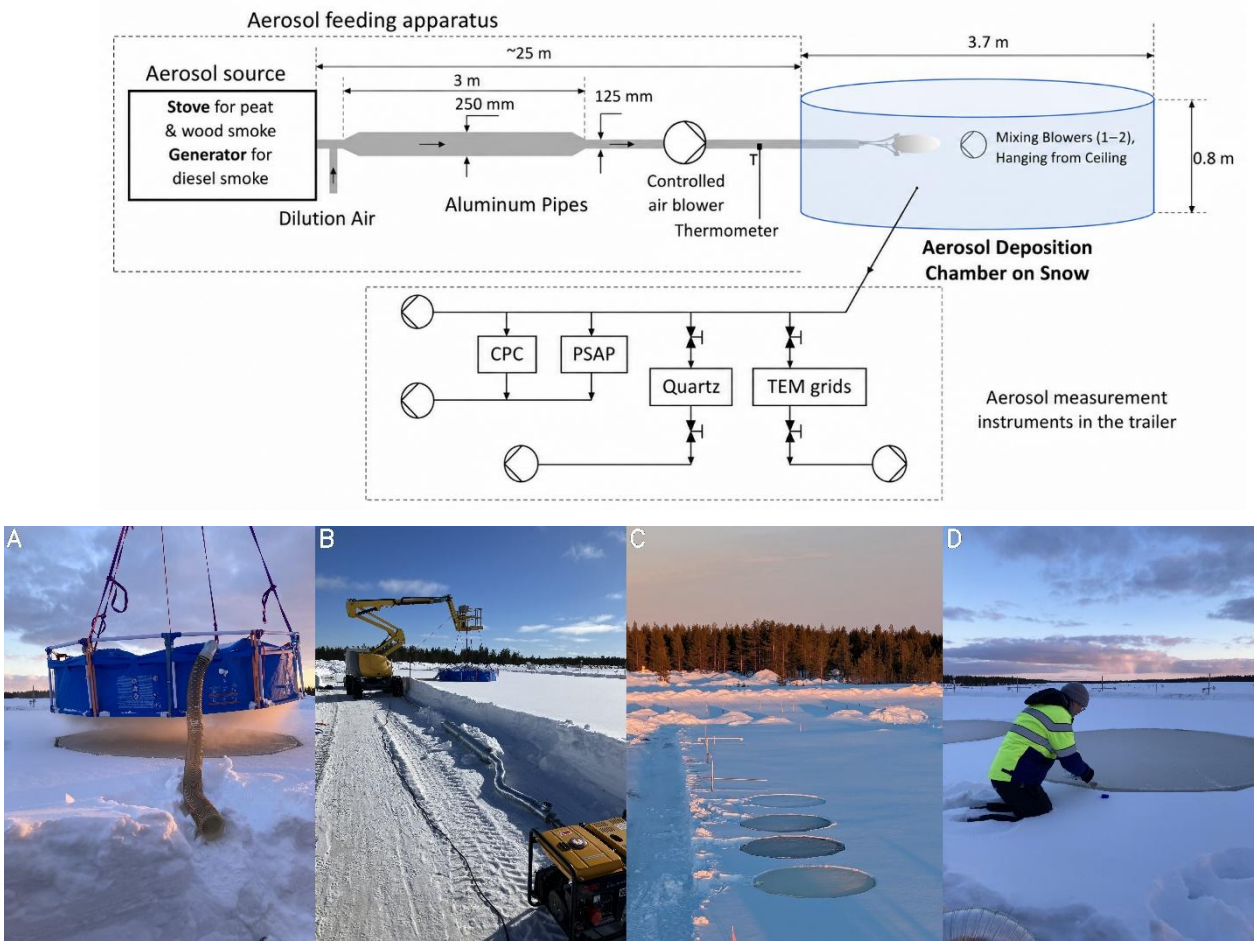


Figure 1. Top panel subfigure: Schematics of the aerosol feeding apparatus, the deposition chamber and aerosol measurement instruments. Bottom panel: Images of subfigures: (A) chamber being lifted after deposition of birch combustion smoke, (B) smoke deposition setup, (C) view of contaminated snow plots, and (D) collection of fresh birch-contaminated snow samples.

Our SoS 2023 campaign focused on light-absorbing carbon particles produced by the combustion of biomass fuels, instead of mechanically-dispersed soot used in earlier campaigns. Light-absorbing carbon particles were generated on-site from birch wood and peat combustion, and the emissions were introduced into the deposition chamber to contaminate the natural snow. The deposition chamber was a sealed cylinder structure (d = 3.7 m, h = 0.8 m) with an open bottom. This chamber was placed on top of untouched natural snow with the chamber hanging from a lifting crane. Birch and peat smoke were produced by burning commercially available birch wood and peat pellets. To prevent melting of the snow during the deposition process,

https://doi.org/10.5194/egusphere-2026-6632
Preprint. Discussion started: 19 November 2026
© Author(s) 2026. CC BY 4.0 License.

the hot combustion exhaust was first led through snow-covered aluminium pipes, cooling it to ~0 °C before entering the chamber placed on top of the snowpack. After deposition, the chamber was lifted and the contaminated snow was exposed to natural meteorological conditions (description in Fig. S1), enabling us to follow post-depositional evolution *in situ*. During the combustion of the peat and birch fuels in the field, aerosol filter samples were collected from inside the deposition chamber via aerosol sampling line, to characterize the optical properties of light-absorbing carbon in the aerosol phase. For comparison with the aerosol-phase, snow samples were collected immediately after particle deposition to determine the corresponding particle properties in freshly contaminated snow.

To follow the temporal and vertical evolution of snow contamination over the melt season, i.e., redistribution and modification of particles within the snowpack during snow metamorphism and melt, snow was repeatedly sampled from both the surface and within the snowpack of the contaminated and an un-contaminated reference snow area. Separate snowpits were prepared at each deposition plot for repeated vertical sampling: the reference pit was established on 24 March 2023, the birch-contaminated pit on 27 March 2023, and the peat-contaminated pit on 28 March 2023. Snow samples were collected with a density cutter and transferred in a frozen state to a freezer prior to particulate carbon measurement. Altogether 66 surface and vertical snow samples were collected with 20 from birch combustion-contaminated plots, 29 from peat combustion-contaminated plots, and 17 from reference plots. Additionally, 7 aerosol samples were collected during the combustion of birch and peat fuels.

Sampling was conducted from the side of each snowpit to minimise exposure of the sampled profile to direct solar radiation and thereby reduce local heating and melting at and near the pit wall. After each sampling event, a styrofoam plate was placed against the exposed pit wall and the pit was refilled with snow to further limit radiative heating, preserve the temperature profile, and minimise disturbance of snow metamorphism between visits. For each snowpit measurement, the microphysical properties of snow were observed to document changes in snow physical state that can influence vertical transport and optical evolution.

The campaign ran from late March until melt out in late April 2023. When the contaminated plots were created from March 24 to 28, daily average temperatures were colder than −10°C at the FMI Sodankylä-Tähtelä observatory 3.6 km south of the SoS site (Fig. S1a). The snow completely disappeared from the contaminated snow plots by the end of April and thereby the entire experiment lasted approximately 30 days, from March 27 to April 28, but snow samples were collected only until April 15. During the snow sampling period the mean daily temperature was -3.5 °C with highest temperature of 10°C and lowest of -29°C. Most days were sunny with little cloud cover (Fig. S1), and the only precipitation occurred as snowfall within a few days after the contaminated snow plots were established. As melting progressed, the snowpacks gradually approached near-isothermal conditions before eventually melting completely.

https://doi.org/10.5194/egusphere-2026-6632
Preprint. Discussion started: 19 November 2026
© Author(s) 2026. CC BY 4.0 License.

2.2 Black carbon and brown carbon quantification

BrC in snow is operationally defined based on solvent solubility and light absorption, because a single standardised method for its quantification has not yet been established. In this study, sequential water-methanol extraction was used to separate WS-BrC and MS-BrC consistently for both aerosol filter samples and snow-derived samples. AAE and MAC were used to provide complementary information on the optical properties of these fractions. AAE describes the wavelength dependence of absorption, whereas MAC represents the mass absorption cross-section. Neither parameter uniquely determines combustion conditions, but both were considered alongside EC/OC ratios and visual observations when interpreting differences in the composition and optical character of the combustion emissions.

The terminology of light-absorbing carbonaceous particles has been discussed extensively in previous studies (e.g., Andreae and Gelencsér, 2006; Bond et al., 2013; Petzold et al., 2013). Bond et al. (2013) identified four characteristic properties of BC: strongly absorbing at visible wavelengths, refractory, insoluble, and composed of aggregates of small carbon spherules. In the present study, the carbonaceous material remaining on the filters after removal of water and methanol-soluble compounds exhibited strong light absorption. Scanning electron microscopy (SEM) analysis of selected aerosol and snow samples revealed aggregates of small carbon spherules in birch-smoke samples, whereas such aggregates were not observed in the examined peat-smoke samples (Norvapalo, 2024). However, the refractoriness of these particles could not be independently verified. Therefore, for the purposes of this study, we operationally refer to the remaining light-absorbing, solvent-insoluble material as BC, using EC mass measured by thermo-optical OCEC analysis as a proxy for BC mass (Birch & Cary 1996), and the absorption spectra measured from the filters to estimate its light absorption. The optical properties of the soluble BrC fractions were determined from ultraviolet–visible (UV-vis) absorption measurements. This approach allowed BrC and BC to be characterised using consistent carbon mass and optical measurements before and after deposition onto snow. Carbonaceous fractions were here quantified using a seven-wavelength DRI thermo-optical OCEC analyser (Chen et al., 2015) with EUSAAR_2 thermal protocol (Cavalli et al., 2010). UV–vis absorption of extracts was measured using a liquid waveguide capillary cell (LWCC-3100, World Precision Instruments) coupled to a UV–vis spectrometer (FLAME-T-UV-VIS-ES, Ocean Optics) and a halogen light source (HL-2000, Ocean Optics). The same spectrometer was used also for measuring absorption through the filter samples by placing the sample in an FHS-UV (Ocean Optics) inline filter holder connected to the light source and the spectrometer with optical fibres.

BrC can be separated into solvent-soluble fractions, and depending on source and solvent, up to about 70% of BrC aerosol mass can be dissolved in water while as much as 90% can be dissolved in methanol (Liu et al., 2013; Laskin et al., 2015; Philips and Smith, 2017; Huang et al., 2020). Methanol is generally more effective than water at extracting a broader range of chromophoric compounds and particularly less polar compounds. To maintain consistency between matrices and avoid ambiguity in fraction definitions, aerosol filter samples were first extracted with Milli-Q water to isolate WS-BrC, and then

https://doi.org/10.5194/egusphere-2026-6632
Preprint. Discussion started: 19 November 2026
© Author(s) 2026. CC BY 4.0 License.



further extracted with methanol to recover MS-BrC from the remaining water-insoluble material. This sequence ensures that the methanol-extracted fraction represents material that is methanol soluble but not water soluble. This approach differs from typical single-step protocols where methanol is applied directly to untreated filters, which can yield overlapping solubility fractions and less comparable MAC values due to co-extraction (Zhu et al., 2018; Bai et al., 2020).

Table 1. Measurements for each snow sample: Optical properties were measured for the melt water (WS-BrC), the filter sample of melt water (Untreated), and for MS-BrC extracted as methanol extract from the untreated filter. Mass of MS-BrC and EC were estimated from OCEC analysis results for Untreated and Treated filters.

Name	Type	Constituents	Analysis	Measured parameters (units)	Info
WS-BrC	Liquid	WS-BrC	Absorption	$b_{abs}(\mathrm{Mm}^{-1})$, AAE	Melted snow after filter
Untreated	Filter	MS-BrC + BC + INS-BrC	Absorption + OCEC	$b_{abs}(\mathrm{Mm}^{-1})$, AAE, m ($\mu\mathrm{g/cm}^2$), MAC (m^2/g)	Filter sample of melted snow
MS-BrC	Liquid	MS-BrC	Absorption	$b_{abs}(\mathrm{Mm}^{-1})$, AAE, MAC ($\mathrm{m}^2/\mathrm{g}$), κ, w	Methanol soluble BrC extracted from the untreated filter
Treated	Filter	BC + INS-BrC	Absorption + OCEC	$b_{abs}(\mathrm{Mm}^{-1})$, AAE, m ($\mu\mathrm{g/cm}^2$), MAC (m^2/g)	Methanol treated filter

The collected snow was melted at room temperature, and the resulting meltwater was filtered through pre-baked quartz-fibre filters, separating dissolved material from insoluble particulate matter (Table 1). The filtrate was analysed by UV spectrophotometry to quantify absorption by WS-BrC. The untreated filters, which retained insoluble particulate material including BC and water-insoluble organic material, were analysed for light absorption and mass by OCEC analysis. Thermo-optical OCEC analysis quantifies carbonaceous material by heating filter punches stepwise under inert and oxidising atmospheres and detecting the evolved carbon, allowing organic carbon (OC), elemental carbon (EC), and total carbon (TC) to be determined. In this study, EC was used as the operational mass basis for BC, while TC was used where appropriate to minimise sensitivity to the OC-EC split point. MS-BrC was extracted from the untreated filters using methanol, after the water extraction step. Filters were submerged in methanol and gently mixed on a tube roller to minimise dislodgement of methanol-insoluble particles such as BC, and the methanol extract was collected for spectral analysis. After extraction, filters were dried in a fume hood and analysed again for absorption and for OCEC analysis, allowing changes in optical properties to be linked to removal of methanol-soluble matter. The mass of MSOC was determined from the difference in TC between the untreated and methanol-treated filters, providing the mass basis for calculating MAC for the methanol-soluble fraction.

Direct one-to-one comparison of absorption measurement values across our and previous studies is limited because extraction protocols and operational definitions of “methanol-soluble” and “water-soluble” fractions differ and are not always reported in a fully harmonised manner. For instance, differences in filtration, extraction time, and whether the extraction is performed

https://doi.org/10.5194/egusphere-2026-6632
Preprint. Discussion started: 19 November 2026
© Author(s) 2026. CC BY 4.0 License.

in a single step or sequentially can influence which BrC chromophores are recovered and, consequently, the derived optical parameters. This methodological distinction is important because single-step methanol extraction of untreated material can dissolve a broader set of OC, including species that would otherwise be partitioned into the water-soluble fraction or remain associated with mixed or weakly polar material, thereby tending to recover more light-absorbing material overall (Laskin et al., 2015; Huang et al., 2020). In the present study, MS-BrC refers specifically to compounds that were first insoluble in water and subsequently soluble in methanol, and this sequential approach therefore provides a more selective view of relatively non-polar chromophores. As a result, absolute MAC and AAE derived here should be compared with caution to studies using one-step extraction (Liu et al., 2013; Mukherjee et al., 2025), because differences may reflect extraction selectivity in addition to true differences in source composition or atmospheric/snow processing.

2.3 Calculations of AAE, MAC, and imaginary part of the refractive index from the UV-vis spectrophotometric measurements

Absorbance spectra obtained from the UV–vis measurements were converted into absorption coefficients and mass-normalised optical parameters for comparison between samples. These calculations were applied consistently to WS-BrC and MS-BrC extracts, and the results were used to quantify wavelength dependence, light absorption, and the imaginary part of the refractive index (κ). Before calculation, raw absorbance spectra $A(\lambda)$ were smoothed with Gaussian process and baseline-corrected by subtracting the absorbance (A) at 700-nm wavelength, where BrC absorption was assumed to be negligible. The absorption coefficient ($b_{abs,}$ in units of m^{-1}) of the liquid extract was then calculated as

$$b_{\mathrm{abs}}\ (\lambda) = (A(\lambda) - A(700\ \mathrm{nm}))\frac{\ln(10)}{L_{LWCC}} \quad (1)$$

where A is the absorbance and L_{LWCC} refers the LWCC optical path length (m) (Hecobain et al., 2010). For methanol extracts, the measured absorbance depends on the amount of melted snow filtered through the corresponding quartz filter. To enable comparison between samples that differ in filtered melt volume, we additionally report a volume-normalised methanol-extract absorption coefficient $b_{\mathrm{abs_MS\text{-}BrC,\ norm}}\ (\mathrm{m}^{-1})$,

$$b_{\mathrm{abs_MS\text{-}BrC,\ norm}}\ (\lambda) = \frac{b_{\mathrm{abs}}(\lambda)\times V_{\mathrm{meoh}}}{V_{\mathrm{melt}}}, \quad (2)$$

where V_{melt} is the filtered meltwater volume (mL) and V_{meoh} methanol solvent volume (mL) used to extract MS-BrC. This normalisation provides an operational measure of absorption per processed snow volume for the methanol-soluble fraction.

The wavelength dependence of absorption was characterised using the AAE, calculated between two wavelengths λ_1 and λ_2 as a power-law slope (e.g., Moosmüller et al., 2011):

$$\mathrm{AAE} = -\frac{\ln(b_{\mathrm{abs}}(\lambda_1)/b_{\mathrm{abs}}(\lambda_2))}{\ln(\lambda_1/\lambda_2)}. \quad (3)$$

Because BrC absorbs strongly in the near-ultraviolet, changes in AAE provide a simple indicator of shifts in spectral shape that can accompany photochemical processing and compositional evolution. Where relevant, AAE was computed using

https://doi.org/10.5194/egusphere-2026-6632
Preprint. Discussion started: 19 November 2026
© Author(s) 2026. CC BY 4.0 License.

multiple wavelength pairs to assess whether changes were more pronounced in the near-ultraviolet or extended into the visible range compared to a simple single-AAE power-law dependence.

Carbon mass associated with the methanol-soluble organic fraction (m_{MSOC}) was derived from thermo-optical analysis by difference, using total carbon to minimise sensitivity to the OC-EC split point and potential pyrolysis artefacts. Specifically, m_{MSOC} was estimated as

$$m_{\mathrm{MSOC}} = (TC_{\mathrm{untreated}} - TC_{\mathrm{methanol\ treated}}) \cdot A_{\mathrm{filter}}\,, \tag{4}$$

where $TC_{\mathrm{untreated}}$ and $TC_{\mathrm{methanol\ treated}}$ are total carbon mass concentrations (mass/area) measured on the filter before and after methanol extraction, respectively and where A_{filter} is the filter area onto which TC was deposited. This approach yields the carbon mass removed by methanol, which is then used as the mass basis for absorption normalisation of the methanol-soluble fraction.

Solution based mass absorption measurements are not directly comparable to filter or aerosol measurements. For dissolved aerosols in solution, the mass absorption coefficient $\mathrm{MAC}_{\mathrm{MS\text{-}BrC}}$ was computed from absorbance (A), path length (l), and carbon concentration in the extract solution as

$$\mathrm{MAC}_{\mathrm{MS-BrC}}(\lambda) = \frac{A(\lambda)}{C \cdot L_{LWCC}} \cdot \ln(10), \tag{5}$$

where C is concentration of MSOC in methanol solution (Hu et al., 2018). For filter-based absorption, the corresponding mass-normalised quantity for EC was calculated using the carbon loading derived from thermo-optical total on the analysed filter punch,

$$\mathrm{MAC}_{\mathrm{BC}}(\lambda) = \frac{b_{\mathrm{abs,\ treated\ filter}}(\lambda)}{\mathrm{EC}}, \tag{6}$$

where $b_{\mathrm{abs,\ treated\ filter}}$ is the measured absorption coefficient assigned to the treated filter sample and EC the elemental carbon mass concentration of the filtered sample. This provides a consistent mass-normalised optical metric for comparing extract-based and filter-based absorption when the mass basis is defined operationally.

The imaginary part κ of the refractive index was estimated from mass absorption coefficient as

$$\kappa(\lambda) = \frac{\mathrm{MAC}\,(\lambda) \cdot \rho \cdot \lambda}{4\pi}, \tag{7}$$

where ρ is particle mass density (Jennings et al., 1979). We used $\rho = 1.4\ \mathrm{g\ cm^{-3}}$ following previous studies (Geller et al., 2006; Mukherjee et al., 2025), noting that $\kappa(\lambda)$ scales linearly with the assumed density and therefore represents an estimate rather than a directly measured quantity. BrC can be classified optically by utilising the wavelength dependence, w, that is related to both MAC and AAE (Saleh et al., 2014, 2020) and $\kappa_{550\mathrm{nm}}$ pair, where w can be estimated with AAE,

$$\mathrm{AAE} \approx w + 1, \tag{8}$$

https://doi.org/10.5194/egusphere-2026-6632
Preprint. Discussion started: 19 November 2026
© Author(s) 2026. CC BY 4.0 License.

To describe vertical redistribution, carbon mass in each sampled layer was expressed as a fraction of the profile-integrated carbon mass for a given sampling date:

$$f_{\mathrm{TC},n} = \frac{TC_{layer,n}}{\sum TC_{layer,n}}, \quad (9)$$

where $\mathrm{TC}_{\mathrm{layer},n}$ is the layer total carbon for layer n expressed on a consistent area (and, where applicable, melt-volume) basis. Contributions of WS-BrC, MS-BrC, and the non-soluble carbon (NSC; carbon non-soluble in water and methanol) fraction, to total absorption were estimated by summing their absorption optical depth τ (or absorbance A) on a common basis:

$$\tau_{\mathrm{tot}}(\lambda) = \tau_{\mathrm{WSOC}}(\lambda) + \tau_{\mathrm{MSOC}}(\lambda) + \tau_{\mathrm{NSC}}(\lambda) \quad (10)$$

For liquid extracts, τ was obtained directly from the LWCC-derived absorption coefficient as $\tau = L_{LWCC}\, b_{abs}$, while the NSC term was derived from absorption measured on the methanol-treated filters and scaled to the corresponding sampled snow volume and analysed filter area, ensuring that all terms represent comparable contributions to the total absorption budget. The absorption optical depth equals the product of absorption coefficient b_{abs} and the length of the absorption path which here $\mathrm{L}_{\mathrm{LWCC}}$ was the length of the LWCC, so

$$b_{\mathrm{abs}} = \tau_{\mathrm{abs}}/L_{LWCC} \quad (1)$$

3 Results and discussion

Here, we first compare BrC optical properties in the aerosol phase and shortly after deposition onto snow (Sect. 3.1). We then examine the temporal evolution of surface-snow BrC optical properties and BC MAC, together with changes in the contributions of carbonaceous fractions to total absorption (Sect. 3.2). Finally, we examine the evolution of BrC optical properties within the snowpack, followed by the vertical redistribution of BrC and birch-derived BC (Sect. 3.3). These results are interpreted in relation to post-depositional aging, snow metamorphism, and melt.

3.1 BrC optical properties in the aerosol phase and after deposition onto snow

After the deposition of the birch and peat combustion-derived emissions onto snow, both contaminated surfaces appeared visually homogeneous, indicating relatively even particle deposition within the treated areas (Fig. S2). The combustion regime was not quantified directly during the experimental burning, and therefore the terms flaming-dominated and smouldering-dominated are used as observational descriptors of the assumed combustion phase. Birch combustion visually appeared more flaming-dominated, as it produced darker smoke, and produced a dark grey snow plot immediately after deposition. In contrast, peat combustion appeared more smouldering-dominated, as it produced little to no visible flame, generated yellow to light-brown smoke, and resulted in a visibly bright yellow snow plot immediately after deposition. Thus, we infer that the birch and peat fuels combusted with different efficiency due to the material's inherent characteristics (Ruppel et al., 2026), that favoured more pronounced EC production for the flaming-dominated birch combustion than the smouldering-dominated peat combustion during our experiment. The aerosol EC/OC ratios of 0.2±0.02 for birch and 0.01±0.001 for peat support this

https://doi.org/10.5194/egusphere-2026-6632
Preprint. Discussion started: 19 November 2026
© Author(s) 2026. CC BY 4.0 License.

conclusion with EC production being more prevalent in flaming-dominated combustion compared to smouldering combustion (McMeeking et al., 2009; Ruppel et al., 2026).

The optical properties of WS-BrC and MS-BrC in the fresh aerosol phase and in snow approximately two hours after deposition are summarised in Table 2. In the fresh aerosol phase, WS-AAE ranged from 9.50 to 9.94, MS-AAE from 4.26 to 5.62, and MS-BrC MAC from 0.49 to 1.24 $m^2\ g^{-1}$. After deposition onto snow, WS-AAE ranged from 8.46 to 9.37, MS-AAE from 5.01 to 5.33, and MS-BrC MAC from 0.41 to 2.12 $m^2\ g^{-1}$. The variations of WS-AAE and MS-AAE with fuel (birch vs. peat) and deposition state (airborne vs. in-snow) were statistically insignificant (overlap within one standard deviation) while WS-AAE was consistently larger than MS-AAE. This indicates that AAE alone did not provide a clear separation between the two fuels in the fresh samples or the difference between aerosol and snow samples. By contrast, MS-BrC MAC showed a stronger fuel-dependent response: birch combustion-derived MS-BrC increased from 1.24 ± 0.15 to 2.12 ± 0.28 $m^2\ g^{-1}$ after deposition, whereas peat combustion-derived MS-BrC remained lower and changed only slightly from 0.49 ± 0.07 to 0.41 ± 0.07 $m^2\ g^{-1}$. This suggests that the fuel-dependent difference in MAC was already present in the fresh material and was enhanced for the snow-extracted MS-BrC fraction.

Table 2. Optical properties of water-soluble and methanol-soluble BrC measured in the aerosol phase (filter samples collected during combustion) and in snow two hours after deposition. AAE values were calculated over 370–470 nm, and MS-BrC MAC at 370 nm. Values are reported as mean ± one standard error.

Combustion type	Condition	WS-AAE (370-470 nm)	MS-AAE (370-470 nm)	MAC ($m^2\ g^{-1}$) (370 nm)
Birch	Fresh airborne	9.94 ± 0.78	4.26 ± 0.67	1.24 ± 0.15
	In-snow, 2 h	9.37 ± 0.83	5.33 ± 0.71	2.12 ± 0.28
Peat	Fresh airborne	9.50 ± 0.69	5.62 ± 0.83	0.49 ± 0.07
	In-snow, 2 h	8.46 ± 0.79	5.01 ± 1.00	0.41 ± 0.07

The measured values fall within the range of previously reported BrC optical properties, although direct comparison across studies is limited by differences in fuel type, wavelength interval, and extraction approach. Ambient studies have reported WS-AAE values of ~3.5–10, MS-AAE values of ~3.1–9.16, and MAC values for methanol-extracted BrC of ~0.14–2.44 $m^2\ g^{-1}$ (Shen et al., 2017; Yan et al., 2020; Zhu et al., 2024). Laboratory biomass-combustion experiments have reported WS-AAE values of 4.4–5.3, MS-AAE values of 4.7–6.2, and MAC values of 0.56–1.38 $m^2\ g^{-1}$ (Mukherjee et al., 2025). In snow studies, WS-AAE values between 1.05 and 6.1 have been reported (Yan et al., 2016; Hu et al., 2018; Zhang et al., 2019), although those values often reflect different extraction procedures and may include more aged or environmentally processed materials.

https://doi.org/10.5194/egusphere-2026-6632
Preprint. Discussion started: 19 November 2026
© Author(s) 2026. CC BY 4.0 License.

The contrast between the two combustion fuels measured here was more clearly reflected by the observed MAC than by AAE. In the fresh aerosol samples, MS-BrC MAC was 1.24 ± 0.15 $m^2 g^{-1}$ for birch and 0.49 ± 0.07 $m^2 g^{-1}$ for peat, while laboratory biomass-combustion experiments have similarly reported lower MAC under smouldering-dominant than flaming-dominant conditions (0.88 and 1.38 $m^2 g^{-1}$, respectively; Mukherjee et al., 2025). Together, the MAC values, EC/OC ratios, and visual observations indicate that birch and peat combustion produced optically and compositionally distinct carbonaceous emissions, with a greater EC contribution under the more flaming-dominant birch combustion conditions. The small differences between aerosol-phase and freshly deposited snow optical properties may reflect changes in partitioning or extractability following deposition onto the snow matrix. However, because the AAE values overlapped within one standard deviation, these changes cannot be clearly distinguished from measurement variability and should not be interpreted as evidence of rapid photochemical aging.

3.2 Temporal evolution of BrC optics at the snow surface

3.2.1 Temporal evolution of BrC AAE

Temporal changes in surface-snow AAE were evaluated for both WS-BrC and MS-BrC at the birch- and peat combustion-contaminated plots during the snowmelt observation period (Fig. 2). The AAE of WS-BrC decreased with time for both combustion fuels, declining from ~9 to 6 within the first two weeks at the peat plot and showing a similar overall decrease at the birch plot. In contrast, the temporal evolution of MS-BrC differed between the birch and peat combustion contaminated plots. At the birch plot, MS-BrC AAE decreased from 5.6 to 4.8, showing weak evidence of a decreasing trend ($p = 0.10$), whereas at the peat plot it increased from 5.0 to 6.6, with similarly weak evidence of an increasing trend ($p = 0.07$). Neither MS-BrC trend reached the conventional $p < 0.05$ significance level, but their opposing directions suggest fuel-dependent differences in the optical evolution of the methanol-soluble fraction.

https://doi.org/10.5194/egusphere-2026-6632
Preprint. Discussion started: 19 November 2026
© Author(s) 2026. CC BY 4.0 License.

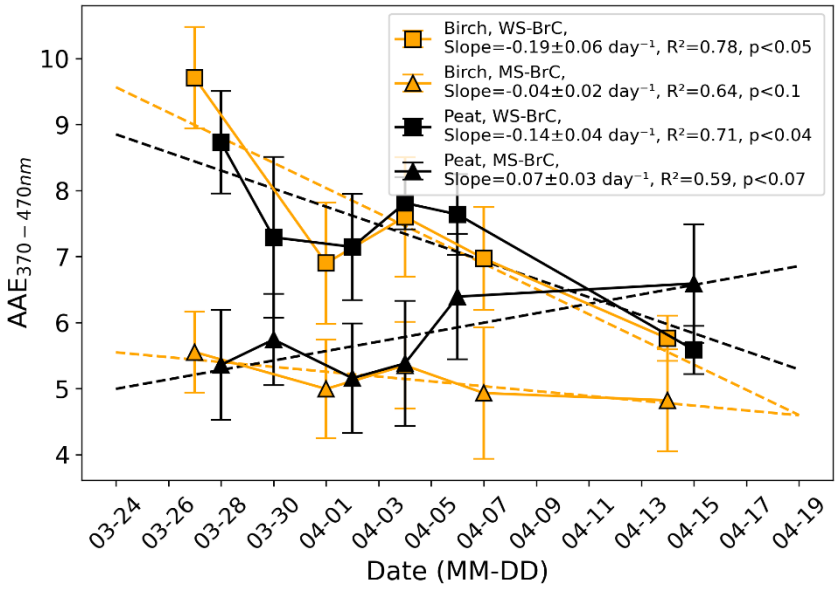


Figure 2. Temporal evolution of the AAE calculated over 370-470 nm for surface snow in the birch (orange) and peat (black) snowpits. Squares represent the WS-BrC fraction and triangles represent the MS-BrC fraction. Dashed black lines show linear regressions, with regression statistics reported in the legend.

A comparable controlled field experiment was conducted by Beres et al. (2020), where particles emitted by smouldering Alaskan boreal peat combustion were deposited onto natural snow. They reported BrC AAE values of 4.86–9.79 over 330–400 nm, overlapping those observed for WS-BrC and MS-BrC in the present study. Comparable values have also been reported for solvent-extracted ambient aerosol, with mean AAE values of ~6–8 depending on wavelength range (Phillips and Smith, 2017; Zhu et al., 2018; Hu et al., 2018). By contrast, filter-based measurements of natural snow have yielded AAE values of 1.5–4 over 450–600 nm across the Arctic and northern China (Doherty et al., 2010; Wang et al., 2013). These lower values represent the combined absorption of BC and other water-insoluble light-absorbing particles retained on filters, rather than isolated BrC fractions. Differences in particle composition, analytical approach, and wavelength interval therefore limit direct comparisons between these measurements and our results. Beyond the agreement in AAE magnitude with previous BrC measurements, our study follows both WS-BrC and MS-BrC over three weeks after a known deposition event. This provides additional insight into their temporal optical evolution during snowmelt and how it differs between soluble fractions and combusted material

To further examine the temporal spectral evolution of BrC, AAE was calculated using several wavelength pairs (Fig. S3). For birch combustion-derived MS-BrC, AAE calculated between 370 and 470 nm decreased modestly with time, whereas values calculated from the longer-wavelength pairs of 400–470 nm and 470–550 nm remained comparatively stable. This pattern suggests that changes were concentrated more strongly in chromophores absorbing at near-UV and ultraviolet wavelengths,

https://doi.org/10.5194/egusphere-2026-6632
Preprint. Discussion started: 19 November 2026
© Author(s) 2026. CC BY 4.0 License.

while compounds contributing to absorption at longer visible wavelengths were comparatively more persistent. Peat combustion-derived MS-BrC showed a more variable pattern, with an initial decrease in AAE followed by a temporary increase and a subsequent decline. Such non-monotonic behaviour suggests that photobleaching may have occurred concurrently with other photochemical processes, such as oxidation, transformation of existing chromophores, or formation of new light-absorbing products (e.g. nitroaromatics and phenolics), resulting in a variable net effect on the spectral shape (Li et al., 2020; Arciva et al., 2024). The contaminated snow plots were exposed to direct and diffuse sunlight starting at the day of deposition, and cloud cover remained generally low during much of the observation period (Fig. S1). The sustained exposure to solar radiation, together with the declining WS-BrC AAE and preferential changes at shorter wavelengths, suggest that photochemical bleaching contributed to the observed optical aging, although its magnitude and evolution differed between the birch and peat combustion-derived BrC due to variable inherent characteristics of the burned fuels (Ruppel et al., 2026).

3.2.2 Temporal evolution of MS-BrC MAC and refractive index κ

The absorption of surface-snow MS-BrC decreased over the observation period, with both MAC at 370 nm and the corresponding imaginary part of the refractive index, κ, showing lower values after three weeks (Fig. 3). MAC at 370 nm decreased from 2.0 to 1.2 $m^2\ g^{-1}$ for birch combustion-derived MS-BrC and from 0.4 to 0.09 $m^2\ g^{-1}$ for peat combustion-derived MS-BrC. The corresponding κ values decreased from 0.08 to 0.055 for birch-derived MS-BrC and from 0.02 to 0.006 for peat-derived MS-BrC. Overall, both metrics indicate systematically weaker absorption for peat-derived BrC than for birch-derived BrC throughout the observation period. BC itself is not expected to undergo the same photochemical bleaching as BrC because its absorption is primarily associated with refractory elemental carbon rather than organic chromophores, although its apparent optical properties can still be affected by changes in mixing state and coatings. Therefore, this subsection focuses on the time-dependent optical evolution of MS-BrC.

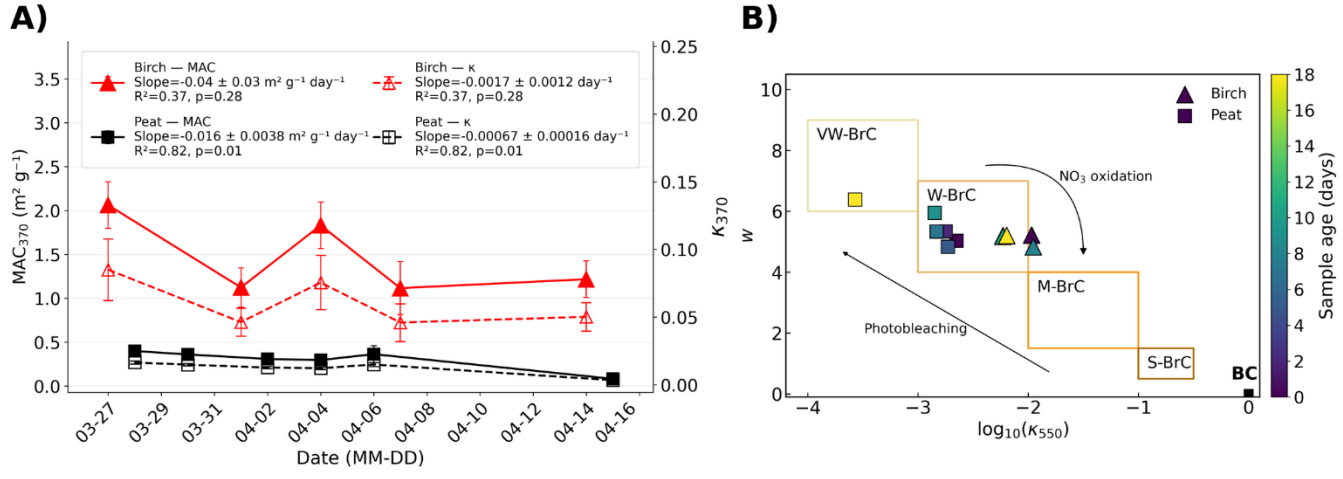
Reported MAC values for BrC show wide variability across studies, reflecting differences in wavelength, extraction protocol, chemical composition, and aging conditions. Chamber experiments have reported fresh MS-BrC MAC values of ~0.46–1.48 $m^2\ g^{-1}$, with aged values between ~0.1–2 $m^2\ g^{-1}$ depending on the combustion fuel and particle aging pathway (Mukherjee et al., 2025). To our knowledge, comparable MAC values specific for snow MS-BrC have rarely been reported, but our MAC values for WS-BrC in snow provide useful context for the magnitude of BrC absorption in snow samples. Reported WS-BrC MAC values include 4.71 ± 3.68 $m^2\ g^{-1}$ around the Tibetan Plateau (Hu et al., 2018), 0.45 ± 0.35 $m^2\ g^{-1}$ in the Altai Mountains (Zhang et al., 2019), and 1.4 ± 0.4 $m^2\ g^{-1}$ in Tibetan glacier snow (Yan et al., 2016). These values provide context for our MAC at 370 nm ranges of 1.2–2.0 $m^2\ g^{-1}$ for birch combustion-derived MS-BrC and 0.09–0.4 $m^2\ g^{-1}$ for peat combustion-derived MS-BrC, although direct comparison should consider differences in wavelength and extraction approach.

https://doi.org/10.5194/egusphere-2026-6632
Preprint. Discussion started: 19 November 2026
© Author(s) 2026. CC BY 4.0 License.

The consistently higher MAC at 370 nm values for birch combustion-derived MS-BrC indicate that the stronger absorption observed in the fresh samples persisted during aging in the snow surface layer. This fuel-dependent contrast is consistent with the differences related to the dominant combustion phase. Thus, although particles produced by the combustion of both fuels showed decreasing absorption with time, the absolute absorption strength of the methanol-soluble fraction remained higher for birch combustion-derived MS-BrC than for peat combustion-derived MS-BrC throughout the observation period.

The derived κ values at 370 nm provide an additional way to compare the absorption of MS-BrC with previous ambient and laboratory studies. Comparable κ values have been reported for biomass burning-derived BrC, although published ranges depend on wavelength, fuel composition, and the method used to derive κ from mass-normalised absorption. For example, κ values of 0.02–0.18 at 365 nm have been observed in the urban Indian Gangetic Plain (Shamjad et al., 2018), 0.008–0.015 for laboratory-generated BrC (Sumlin et al., 2018), and 0.013–0.062 at 405 nm for aerosol filter samples from a North American city (Liu et al., 2015). In laboratory aging chamber experiments, κ at 550 nm for MS-BrC ranged from 0.002 to 0.011 (Mukherjee et al., 2025), which is broadly consistent with the lower end of the values observed here. Because κ is typically inferred from mass-normalised absorption using an assumed particle density, differences in density assumptions and in the operational definition of the extracted fraction can shift reported values even for similar fuel types.

The optical "brownness" of BrC can be interpreted using the κ–w pair, where κ at 550 nm (κ_{550}) describes absorption strength and w describes wavelength dependence (Eq. 8). More strongly absorbing BrC is characterised by higher κ_{550} and weaker w, whereas optically weaker BrC has lower κ_{550} and higher w. The classification therefore separates BrC into regions ranging from more strongly absorbing S-BrC to very weakly absorbing VW-BrC (Saleh et al., 2014, 2020). This framework is useful here because it allows the temporal evolution of MS-BrC to be interpreted not only as a change in absorption magnitude, but also as a change in spectral character during aging in the snow surface layer.



https://doi.org/10.5194/egusphere-2026-6632
Preprint. Discussion started: 19 November 2026
© Author(s) 2026. CC BY 4.0 License.

Figure 3. Temporal evolution and optical classification of surface-snow MS-BrC from the birch- and peat-contaminated plots. (A) Time series of MAC at 370 nm and the corresponding κ values on two y-axes. Linear regression slopes are reported in the legend as slope ± standard error, with MAC slopes given in m² g⁻¹ day⁻¹. (B) κ at 550 nm is shown as a function of w, where κ represents absorption strength and w wavelength dependence. The VW-BrC, W-BrC, M-BrC, and S-BrC regions represent very weakly, weakly, moderately, and strongly absorbing BrC classes following Saleh et al. (2014, 2020). Connected points indicate temporal progression during the observation period.

The κ_{550}–w classification indicates that the surface snow MS-BrC samples fall mainly within the W-BrC region (Fig. 3), which is commonly associated with smouldering-derived BrC (Saleh et al., 2014, 2020; Mukherjee et al., 2025). Peat combustion-derived MS-BrC was located almost entirely within the W-BrC region, consistent with the visually smouldering-dominant combustion conditions during peat burning. Birch combustion-derived MS-BrC initially plotted near the transition between W-BrC and M-BrC, indicating stronger absorption that is consistent with the more flaming-dominant combustion characteristics. With increasing sample age, both birch and peat combustion-derived MS-BrC shifted generally toward higher w and lower κ_{550}, approaching the VW-BrC region. This trend suggests progressive photobleaching and compositional aging of MS-BrC in the snow surface layer, consistent with transformation or removal of strongly absorbing chromophores and a shift toward an optically weaker and more strongly wavelength-dependent BrC fraction.

3.2.3 Temporal evolution of BC and contributions of carbonaceous fractions to surface-snow absorption

The MAC of BC derived from methanol-treated filters changed considerably during the observation period at 532, 635, and 780 nm (Fig. 4). At 635 nm, BC MAC decreased from ~17.75 m² g⁻¹ for freshly deposited material to ~4.5 m² g⁻¹ three weeks after deposition. Because BC itself does not undergo photochemical bleaching, this decrease likely reflects changes in the physical or mixing state of BC and/or in the residual material contributing to absorption after extraction rather than degradation of the BC chromophore itself. For instance, changes in aggregation can alter BC MAC through shielding effects within larger particle clusters. This was observed within few days after deposition, as the BC present on the snow surface formed large aggregates that could be observed visually (Figs. S2A-B). The previous SoS campaign (SoS 2018) presented SEM-analyses that indicated the agglomeration of BC particles in the snowpack with time. The methanol-treated peat samples contained very little residual EC and showed negligible absorption, consistent with the substantially smaller BC contribution to particles

https://doi.org/10.5194/egusphere-2026-6632
Preprint. Discussion started: 19 November 2026
© Author(s) 2026. CC BY 4.0 License.

emitted from the predominantly smouldering peat combustion. Consequently, a temporal BC MAC could not be reliably evaluated for the peat plot.

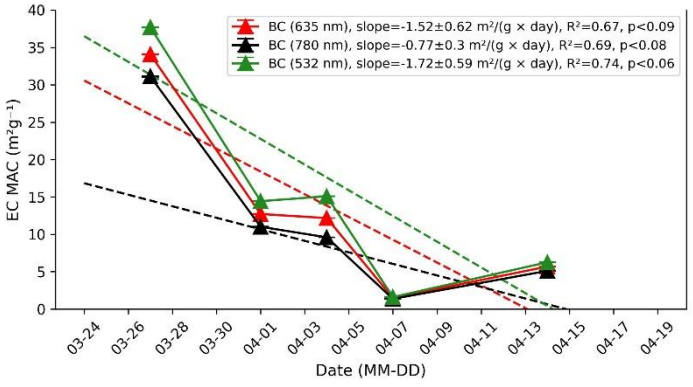


Figure 4. Temporal evolution of surface-snow BC MAC derived from absorption of methanol-treated filters and EC measured by thermo-optical OCEC analysis. MAC values are shown for 532, 635, and 780 nm. Only birch-derived samples are shown because residual EC and absorption in the methanol-treated peat samples were too low for reliable determination of peat BC MAC.

The relative contributions of WS-BrC, MS-BrC, and NSC to total surface snow absorption were estimated using the fraction-resolved approach (Fig. 5). In both contaminated plots, the relative contribution of WS-BrC decreased during the observation period, whereas the contribution of MS-BrC generally increased. The contribution of NSC, which includes BC and organic material insoluble in both water and methanol, remained comparatively stable. The smaller NSC contribution in the peat plot is consistent with its lower EC/OC ratio and weaker contribution from BC compared with the more flaming-dominant birch combustion. These changes show that aging altered not only the magnitude of surface snow absorption but also the relative importance of the different carbonaceous fractions.

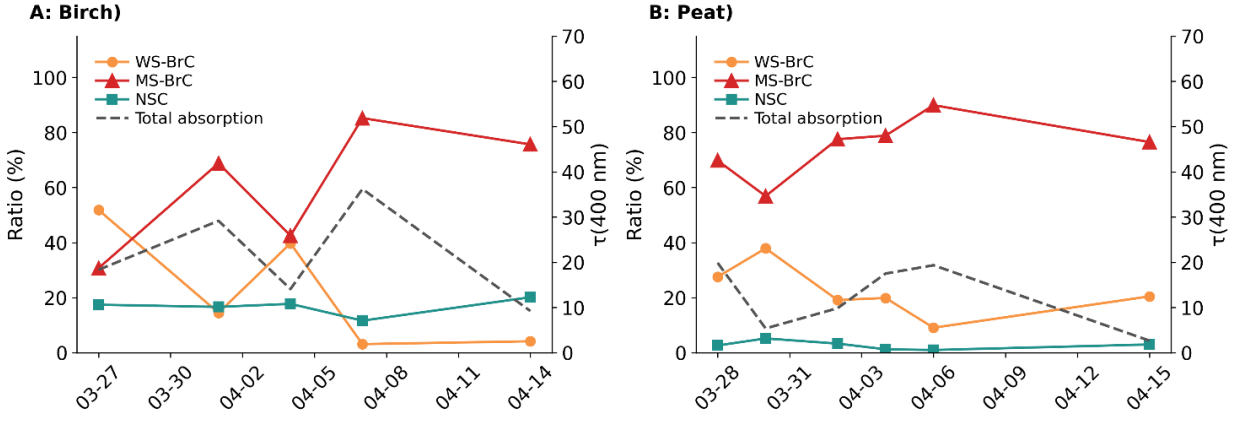


Figure 5. Relative contributions of WS-BrC, MS-BrC, and NSC to total absorption at 400 nm in surface snow from the (A) birch- and (B) peat-contaminated plots. The primary y-axis shows the fractional contribution of each carbonaceous fraction to total absorption, while the secondary y-axis shows total absorption optical depth at 400 nm.

https://doi.org/10.5194/egusphere-2026-6632
Preprint. Discussion started: 19 November 2026
© Author(s) 2026. CC BY 4.0 License.

The temporal evolution of the fraction-resolved absorption indicates that chemical aging and physical redistribution occurred concurrently during snowmelt. The decreasing contribution of WS-BrC, together with the declining surface absorption and WS-BrC AAE, is consistent with photochemical bleaching and preferential removal of water-soluble material with meltwater, analogous to the early elution of soluble impurities during snowmelt (Bales et al., 1989). In contrast, the increasing relative contribution of MS-BrC does not necessarily indicate increasing absolute MS-BrC absorption, but rather that this fraction became relatively more important as WS-BrC was removed or weakened more rapidly. The comparatively stable contribution of NSC suggests greater retention of water- and methanol-insoluble material at the snow surface.

Together, the temporal evolution of AAE, MAC, and the relative absorption contributions shows that the optical properties of BrC in snow depend on both post-depositional processing and fuel composition. AAE may therefore provide a qualitative indicator of the processing state of BrC when the fuel, extracted fraction, and wavelength interval are constrained, but it should not be interpreted as a unique measure of BrC age because selective transport and compositional changes can also alter its spectral dependence. The persistence of elevated AAE and mass-normalised absorption over several weeks further suggests that optically active BrC can persist in snow longer than the characteristic photobleaching timescales reported for airborne BrC, where substantial absorption losses can occur within hours to days (Forrister et al., 2015; Hems et al., 2021). Differences in irradiation, temperature, and the physical environment of particles within the snowpack may contribute to this persistence, although differences in extraction method and wavelength range should also be considered when comparing snow- and aerosol-based measurements.

3.3 Temporal evolution of light-absorbing carbon within the snowpack

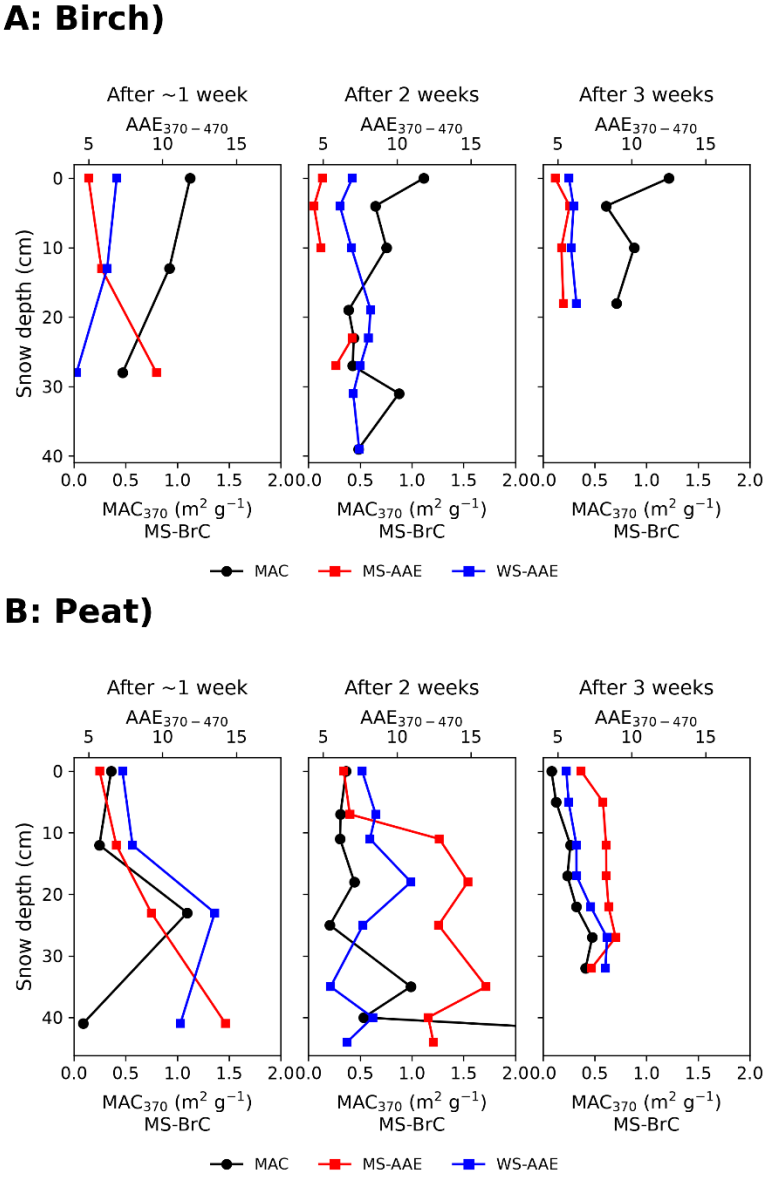
3.3.1 Temporal evolution of BrC optics within the snowpack

The depth-resolved profiles showed that MS-BrC generally exhibited higher AAE below the snow surface, whereas the vertical behaviour of WS-BrC was more variable (Fig. 6). In the birch snowpit after around one week, WS-AAE decreased from ~ 7 at the surface to ~ 4 in the deepest sampled layer. In contrast, MS-AAE increased from ~ 5 to 10 over the same profile. After two weeks, birch WS-AAE generally ranged from 6 to 8, with somewhat higher values at intermediate depths, while the MS-AAE ranged from 4 to 7. By the third week, both fractions showed relatively little variation over the sampled depth range, with MS-AAE around 5–6 and WS-AAE around 6.

The vertical profiles of MS-BrC MAC did not consistently follow those of AAE. In the birch snowpit, surface MAC at 370 nm was 1.1–1.5 $m^2\ g^{-1}$ and was generally higher than the subsurface values, which were mostly around 0.4–0.9 $m^2\ g^{-1}$. In contrast, the peat profile after three weeks showed the lowest MAC at the surface, below ~ 0.1 $m^2\ g^{-1}$, followed by generally

https://doi.org/10.5194/egusphere-2026-6632
Preprint. Discussion started: 19 November 2026
© Author(s) 2026. CC BY 4.0 License.

500 higher values of 0.2–0.5 m² g⁻¹ in the subsurface layers. Relatively low MAC in several deeper layers indicates weaker absorption, even where AAE was elevated.



505 **Figure 6. Vertical profiles of optical properties in the (A) birch and (B) peat snowpit after one, two, and three weeks. Black circles show MAC at 370 nm, and red squares indicates MS-AAE and blue the WS-AAE calculated over 370–470 nm.**

The decreasing WS-AAE with depth in the birch snowpit after the first week may reflect a limited contribution of newly deposited WS-BrC to the deeper sampled layers. If downward redistribution was still limited, the deeper WS-BrC absorption

https://doi.org/10.5194/egusphere-2026-6632
Preprint. Discussion started: 19 November 2026
© Author(s) 2026. CC BY 4.0 License.

could have been more strongly influenced by organic chromophores already present in the snowpack. Such background chromophores have been documented in Arctic snow, where soluble light absorption can arise from several sources rather than from recent combustion deposition alone (Beine et al., 2011). The contrasting WS-AAE and MS-AAE profiles may therefore reflect different contributions of deposited and pre-existing material to the two fractions, rather than differences in post-depositional aging alone. This explanation remains tentative because AAE does not quantify the amount of deposited BrC present in a layer or establish its origin.

Where AAE was lower near the surface than in deeper layers, the pattern is consistent with a contribution from stronger photochemical processing in the upper snowpack. Snow attenuates solar radiation with depth, potentially reducing photochemical exposure in deeper layers (Anastasio et al., 2007). Declining near-surface absorption attributed to photobleaching has been reported in Arctic snow (Beine et al., 2011), while laboratory experiments with aqueous biomass-burning BrC have demonstrated that photochemical changes can reduce AAE through both short-wavelength bleaching and longer-wavelength absorption enhancement (Mukherjee et al., 2025). Consequently, the profiles may reflect a combination of photochemical transformation, selective redistribution and changing contributions from deposited and pre-existing organic material, whose individual effects cannot be separated using the optical measurements alone.

3.3.2 Vertical distribution of BrC within the snowpack

Repeated depth-resolved sampling of WS-BrC and MS-BrC showed distinct changes in their vertical distribution during snowmelt. In both contaminated plots, absorption was initially concentrated near the snow surface during the first week after deposition, whereas absorption in the reference snow remained close to the detection limit throughout the observation period (Figs. 7 and 8). As melting progressed, WS-BrC and MS-BrC showed different vertical behaviour, with redistribution also differing between the birch- and peat-contaminated plots.

Observed ice layers can restrict vertical melt water flow and redirect percolation into preferential pathways within the snowpack, which affects the redistribution of dissolved and particle-bound constituents. Ice layers persisted in the reference snow throughout the observation period (Figs. 7 and 8). In contrast, the contaminated snowpacks approached near-isothermal conditions more than a week earlier than the reference snow. Distinct ice layers were no longer observed after three weeks for the contaminated snow, as a result of substantial snow metamorphism which increases connectivity of meltwater pathways within the snowpack.

In the water-extract profiles, WS-BrC absorption was initially confined mainly to the uppermost snow layers, with the strongest absorption occurring at shorter wavelengths (Fig. 7). As melting progressed, measurable WS-BrC absorption appeared in deeper layers, indicating downward transport of water-soluble light-absorbing material. At the same time, the overall WS-BrC

https://doi.org/10.5194/egusphere-2026-6632
Preprint. Discussion started: 19 November 2026
© Author(s) 2026. CC BY 4.0 License.

absorption signal weakened after two weeks, consistent with a combination of downward flushing and photochemical bleaching at the surface. Absorption detected beneath ice layers suggests that these layers did not completely prevent vertical transport and that preferential meltwater pathways allowed WS-BrC to cross layer boundaries. Downward redistribution became particularly apparent as the contaminated snowpacks approached near-isothermal conditions, when meltwater percolation through the snowpack was likely enhanced (Zhang et al., 2019; Kang et al., 2022).

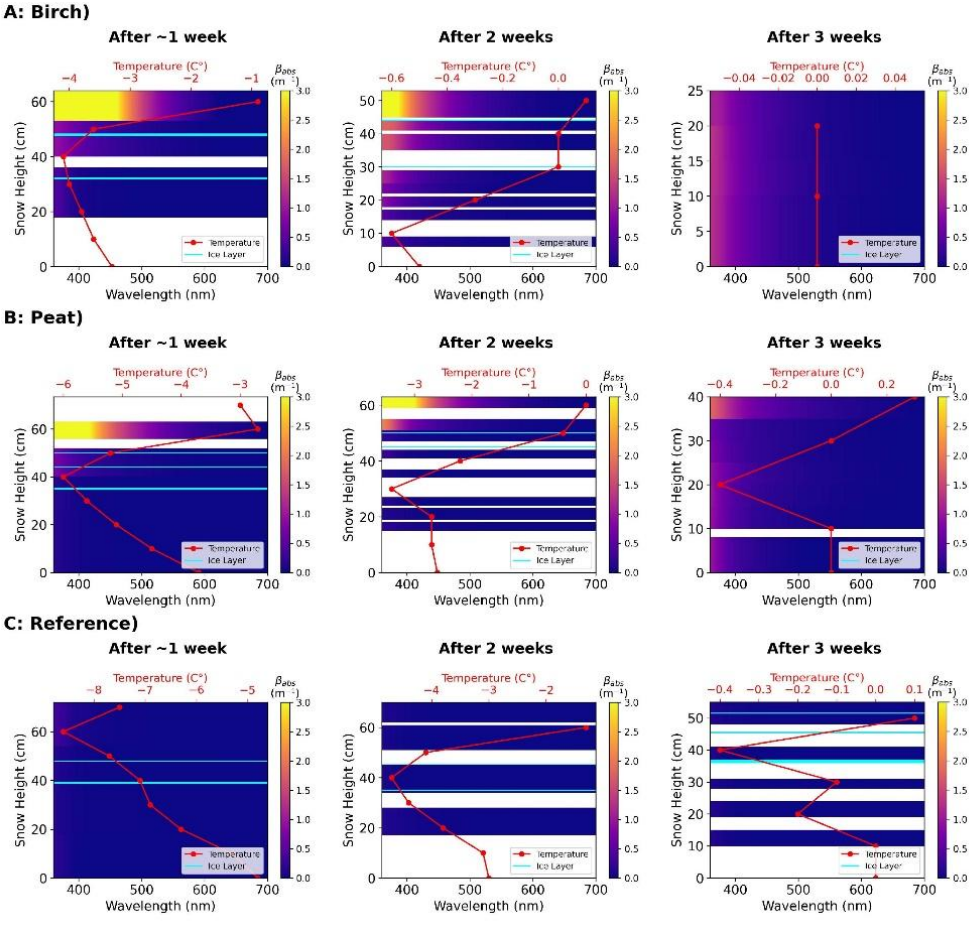


Figure 7. Depth-resolved absorption spectra of water extracts for the snowpits. Heat maps show the absorption coefficient as a function of wavelength and snow height for (A) birch, (B) peat, and (C) reference snow at the sampling dates shown above each panel. Each horizontal band represents a sampled layer. High absorption appears as bright yellow colours, whereas dark blue indicates weak or negligible absorption. Overlaid profiles show snow temperature (solid red) and light-blue horizontal lines indicate observed ice layers.

The methanol-extract profiles showed different behaviour from the water-extract profiles and generally exhibited absorption over a broader wavelength range (Fig. 8). MS-BrC also showed a stronger fuel dependence. Birch combustion-derived MS-BrC remained concentrated near the surface during the early part of the campaign but became detectable in deeper layers as melting progressed and the snowpack approached near-isothermal conditions. In contrast, peat combustion-derived MS-BrC

https://doi.org/10.5194/egusphere-2026-6632
Preprint. Discussion started: 19 November 2026
© Author(s) 2026. CC BY 4.0 License.

remained predominantly concentrated near the surface throughout the sampling period. The delayed appearance of birch combustion-derived MS-BrC at depth is consistent with transport or physical relocation of water-insoluble, particle-associated material through preferential meltwater pathways and melt-driven snow restructuring rather than efficient dissolution into bulk meltwater. This interpretation is consistent with the operational definition of MS-BrC in this study, which represents material retained during water filtration and subsequently extracted with methanol.

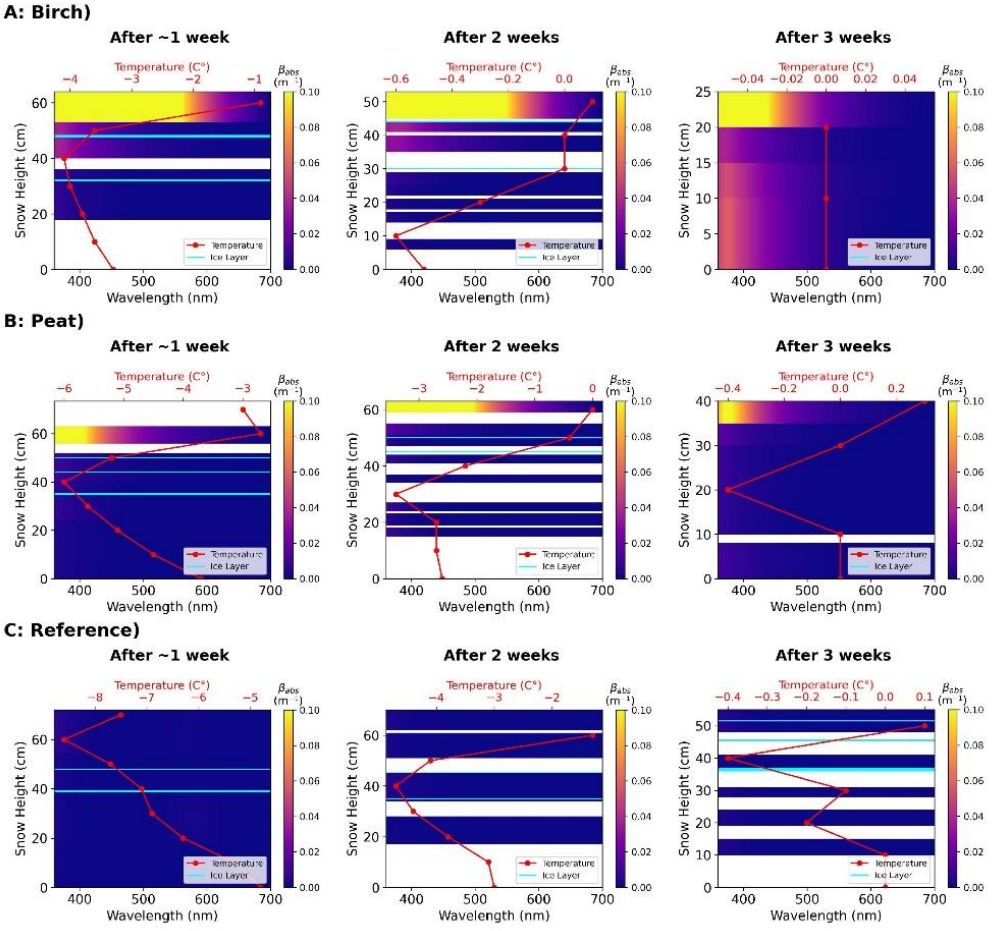


Figure 8. Depth-resolved absorption spectra of methanol extracts for the snowpits for (A) birch, (B) peat, and (C) reference snow at the sampling dates shown above each panel. Figure explanation is the same as in Fig. 7.

The weak absorption observed in deeper snow layers during the first week suggests a limited contribution from newly deposited BrC and affects the interpretation of corresponding AAE values (Fig. 6). At low absorption levels, small absolute uncertainties in absorption at 370 and 470 nm can substantially affect their ratio and the calculated AAE, potentially contributing to the atypical first-week birch WS-AAE profile. By three weeks, increased downward redistribution as the snowpacks approached near-isothermal conditions coincided with more uniform AAE over the sampled depths, particularly in the birch snowpit. This

https://doi.org/10.5194/egusphere-2026-6632
Preprint. Discussion started: 19 November 2026
© Author(s) 2026. CC BY 4.0 License.

may reflect a greater contribution of redistributed BrC to deeper-layer absorption and, where absorption signals became stronger, reduced sensitivity of AAE to measurement uncertainty.

3.3.3. Vertical distribution of BC in birch-smoke contaminated snowpack

BC was substantially more abundant in the birch-contaminated snowpack than in the peat-contaminated snowpack, consistent with the higher EC/OC ratio and more flaming-dominant combustion characteristics observed for the birch-contaminated snowpack. The vertical distribution of birch combustion-derived EC remained concentrated near the snow surface throughout the observation period (Fig. 9). Surface EC concentration was ~0.05 mg L^{-1} one week after deposition, increased to ~0.20 mg L^{-1} after two weeks, and subsequently decreased to ~0.04 mg L^{-1} after three weeks. The increase is consistent with melt-induced surface enrichment of relatively insoluble BC, whereas the subsequent decrease suggests redistribution or removal of BC from the surface layer as melting or should it be that melting was enhanced, a similar pattern which was observed in earlier SoS campaigns (Svensson et al., 2024).

The EC/OC ratio at the surface increased from ~0.05 after one week to ~0.25 after three weeks, indicating preferential loss of OC relative to EC from the surface layer. In deeper snow layers, EC/OC generally remained below 0.05, except after three weeks when values increased to ~0.055–0.088. This coincided with the snowpack approaching near-isothermal conditions and suggests that a fraction of the BC was redistributed into deeper layers during enhanced meltwater transport and snow restructuring. Overall, the vertical profiles indicate that BC was preferentially retained and enriched near the surface during much of the melt period, while only limited transport to deeper layers occurred until the later stages of snowmelt. Similar surface retention and melt amplification of BC have been reported during spring snowmelt in the Sierra Nevada (Chellman et al., 2026).

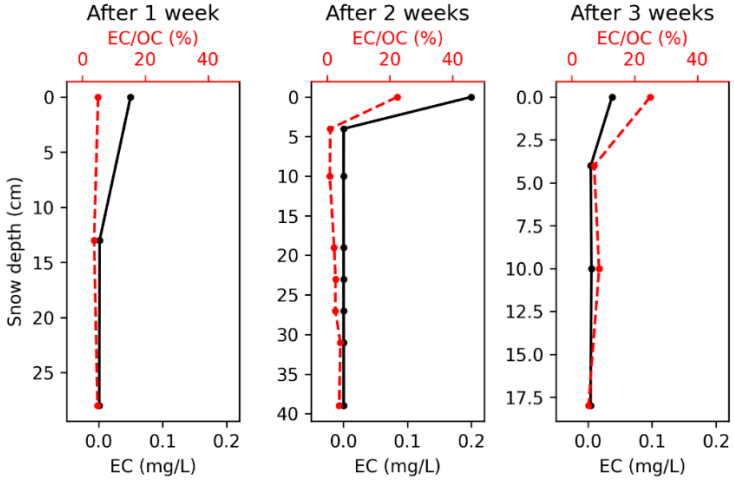


Figure 9. Vertical distribution of EC and EC/OC ratio in birch-smoke contaminated snowpit.

https://doi.org/10.5194/egusphere-2026-6632
Preprint. Discussion started: 19 November 2026
© Author(s) 2026. CC BY 4.0 License.

4 Conclusions

In the controlled SoS 2023 field deposition experiment, birch- and peat-combustion emissions were deposited onto natural snow in subarctic Finland. Repeated surface and depth-resolved samples were collected to investigate changes in the optical properties and redistribution of WS-BrC, MS-BrC, and BC during snowmelt. The results show how these carbonaceous fractions continue to evolve during snow metamorphism and melt. WS-BrC was likely redistributed in dissolved form with percolating meltwater, whereas MS-BrC and BC were retained more strongly near the surface. Some downward redistribution of water-insoluble material became apparent as the snowpack approached near-isothermal condition, particularly for birch-derived MS-BrC and BC, while peat-derived MS-BrC remained mainly near the surface. Birch-derived BC MAC at 635 nm decreased from ~ 17.75 to 4.5 $m^2\ g^{-1}$ over three weeks, where the changes were likely reflected in particle aggregation and mixing state.

WS-BrC showed the clearest temporal change in spectral absorption, with surface snow AAE decreasing from ~ 9 to 6 alongside declining absorption. Across both contaminated snowpits, AAE values for WS-BrC and MS-BrC were generally lower near the surface than in deeper layers. This contrast suggests greater photochemical alteration of BrC in the layers most exposed to sunlight, where preferential transformation or loss of short-wavelength absorbing chromophores could reduce AAE through photobleaching. Selective redistribution of BrC components also contributed to the vertical differences, so the AAE profiles cannot be attributed to photobleaching alone. Meanwhile, the decreasing contribution of WS-BrC and increasing relative contribution of MS-BrC show that post-depositional processing altered the composition of the surface snow absorption budget as well as its magnitude.

Despite these changes, BrC and BC remained optically active throughout the three-week observation period. These findings demonstrate that seasonal snow can act as an evolving optical reservoir, where chemical ageing, surface retention, and meltwater-driven redistribution alter both the magnitude and vertical distribution of light absorption. Consequently, the potential radiative influence of deposited particles may depend not only on their initial properties and concentrations but also on their subsequent evolution within the snowpack. However, the contributions of photochemical processes and physical redistribution could not be independently quantified for their effects on snow albedo and radiative forcing. Future studies should therefore focus on accounting temporal evolution of BC and BrC optical properties and how they affect snow albedo and radiative forcing. Accounting for these post-depositional processes will improve the representation of aerosol-driven snow darkening and its potential climate implications.

https://doi.org/10.5194/egusphere-2026-6632
Preprint. Discussion started: 19 November 2026
© Author(s) 2026. CC BY 4.0 License.

Data availability

All data will be available in the Finnish Meteorological Institute open access data base METIS.

Author contributions

AV designed the experiments and DL, KL, JS, HM, and AV carried them out. Measurements were performed by DL, KL, JS, and IM-A. Data analysis was done by DL, KL, JS, MR, HM, and AV. The manuscript was prepared by DL with help from KL, JS, MR, HM and AV.

Competing interests

The authors declare that they have no conflict of interest.

Acknowledgements

The authors acknowledge the support received during the campaign from Anna Kontu and other staff members of FMI Sodankylä. Olli Sippula for providing peat samples. Oona Norvapalo for various contribution during the measurement campaign.

Financial support

This work has been supported by the Research Council of Finland consortium: “Black and Brown Carbon in the Atmosphere and the Cryosphere” (BBrCAC project no. 341271), and Research Council of Finland project no. 355871.

References

Anastasio, C., Galbavy, E. S., Hutterli, M. A., Burkhart, J. F., and Friel, D. K.: Photoformation of hydroxyl radical on snow grains at Summit, Greenland, Atmospheric Environment, 41, 5110–5121, https://doi.org/10.1016/j.atmosenv.2006.12.011, 2007.

Andreae, M. O. and Gelencsér, A.: Black carbon or brown carbon? The nature of light-absorbing carbonaceous aerosols, Atmospheric Chemistry and Physics, 6, 3131–3148, https://doi.org/10.5194/acp-6-3131-2006, 2006.

Arciva, S., Ma, L., Mavis, C., Guzman, C., and Anastasio, C.: Formation and loss of light absorbance by phenolic aqueous SOA by OH and an organic triplet excited state, Atmospheric Chemistry and Physics, 24, 4473–4485, https://doi.org/10.5194/acp-24-4473-2024, 2024.

https://doi.org/10.5194/egusphere-2026-6632
Preprint. Discussion started: 19 November 2026
© Author(s) 2026. CC BY 4.0 License.

Bai, Z., Zhang, L., Cheng, Y., Zhang, W., Mao, J., Chen, H., Li, L., Wang, L., and Chen, J.: Water/Methanol-Insoluble Brown Carbon Can Dominate Aerosol-Enhanced Light Absorption in Port Cities, Environ. Sci. Technol., 54, 14889–14898, https://doi.org/10.1021/acs.est.0c03844, 2020.

Bales, R. C., Davis, R. E., and Stanley, D. A.: Ion elution through shallow homogeneous snow, Water Resources Research, 25, 1869–1877, https://doi.org/10.1029/WR025i008p01869, 1989.

Barreira, L. M. F., Aurela, M., Saarikoski, S., Li, D., Teinilä, K., Virkkula, A., Niemi, J. V., Manninen, H. E., Pirjola, L., Petäjä, T., Rönkkö, T., and Timonen, H.: Characterizing winter-time brown carbon: Insights into chemical and light-absorption properties in residential and traffic environments, Science of The Total Environment, 955, 177089, https://doi.org/10.1016/j.scitotenv.2024.177089, 2024.

Beine, H., Anastasio, C., Esposito, G., Patten, K., Wilkening, E., Domine, F., Voisin, D., Barret, M., Houdier, S., and Hall, S.: Soluble, light-absorbing species in snow at Barrow, Alaska, Journal of Geophysical Research: Atmospheres, 116, https://doi.org/10.1029/2011JD016181, 2011.

Beres, N. D., Sengupta, D., Samburova, V., Khlystov, A. Y., and Moosmüller, H.: Deposition of brown carbon onto snow: changes in snow optical and radiative properties, Atmospheric Chemistry and Physics, 20, 6095–6114, https://doi.org/10.5194/acp-20-6095-2020, 2020.

Birch, M. E. and Cary, R. A.: Elemental Carbon-Based Method for Monitoring Occupational Exposures to Particulate Diesel Exhaust, Aerosol Science and Technology, 25, 221–241, https://doi.org/10.1080/02786829608965393, 1996.

Bond, T. C., Doherty, S. J., Fahey, D. W., Forster, P. M., Berntsen, T., DeAngelo, B. J., Flanner, M. G., Ghan, S., Kärcher, B., Koch, D., Kinne, S., Kondo, Y., Quinn, P. K., Sarofim, M. C., Schultz, M. G., Schulz, M., Venkataraman, C., Zhang, H., Zhang, S., Bellouin, N., Guttikunda, S. K., Hopke, P. K., Jacobson, M. Z., Kaiser, J. W., Klimont, Z., Lohmann, U., Schwarz, J. P., Shindell, D., Storelvmo, T., Warren, S. G., and Zender, C. S.: Bounding the role of black carbon in the climate system: A scientific assessment, Journal of Geophysical Research: Atmospheres, 118, 5380–5552, https://doi.org/10.1002/jgrd.50171, 2013.

Cavalli, F., Viana, M., Yttri, K. E., Genberg, J., and Putaud, J.-P.: Toward a standardised thermal-optical protocol for measuring atmospheric organic and elemental carbon: the EUSAAR protocol, Atmospheric Measurement Techniques, 3, 79–89, https://doi.org/10.5194/amt-3-79-2010, 2010.

Chellman, N., Ammatelli, J. H., Moosmüller, H., McCrimmon, D., Griessbaum, N., Bair, E. H., Blanchette, C., and Hausner, M.: Light Absorbing Particles Are Retained in Snow During Springtime Snowmelt in the Sierra Nevada, CA, Journal of Geophysical Research: Atmospheres, 131, e2025JD046083, https://doi.org/10.1029/2025JD046083, 2026.

Chen, L.-W. A., Chow, J. C., Wang, X. L., Robles, J. A., Sumlin, B. J., Lowenthal, D. H., Zimmermann, R., and Watson, J. G.: Multi-wavelength optical measurement to enhance thermal/optical analysis for carbonaceous aerosol, Atmospheric Measurement Techniques, 8, 451–461, https://doi.org/10.5194/amt-8-451-2015, 2015.

Doherty, S. J., Warren, S. G., Grenfell, T. C., Clarke, A. D., and Brandt, R. E.: Light-absorbing impurities in Arctic snow, Atmospheric Chemistry and Physics, 10, 11647–11680, https://doi.org/10.5194/acp-10-11647-2010, 2010.

Doherty, S. J., Grenfell, T. C., Forsström, S., Hegg, D. L., Brandt, R. E., and Warren, S. G.: Observed vertical redistribution of black carbon and other insoluble light-absorbing particles in melting snow, Journal of Geophysical Research: Atmospheres, 118, 5553–5569, https://doi.org/10.1002/jgrd.50235, 2013.

https://doi.org/10.5194/egusphere-2026-6632
Preprint. Discussion started: 19 November 2026
© Author(s) 2026. CC BY 4.0 License.

Doherty, S. J., Dang, C., Hegg, D. A., Zhang, R., and Warren, S. G.: Black carbon and other light-absorbing particles in snow of central North America, Journal of Geophysical Research: Atmospheres, 119, 12,807-12,831, https://doi.org/10.1002/2014JD022350, 2014.

Flanner, M. G., Zender, C. S., Randerson, J. T., and Rasch, P. J.: Present-day climate forcing and response from black carbon in snow, Journal of Geophysical Research, 112, https://doi.org/10.1029/2006JD008003, 2007.

Forrister, H., Liu, J., Scheuer, E., Dibb, J., Ziemba, L., Thornhill, K. L., Anderson, B., Diskin, G., Perring, A. E., Schwarz, J. P., Campuzano-Jost, P., Day, D. A., Palm, B. B., Jimenez, J. L., Nenes, A., and Weber, R. J.: Evolution of brown carbon in wildfire plumes, Geophysical Research Letters, 42, 4623–4630, https://doi.org/10.1002/2015GL063897, 2015.

Forster, P., Storelvmo, T., Armour, K., Collins, W., Dufresne, J.-L., Frame, D., Lunt, D. J., Mauritsen, T., Palmer, M. D., Watanabe, M., Wild, M., and Zhang, H.: The Earth's Energy Budget, Climate Feedbacks, and Climate Sensitivity, in: Climate Change 2021: The Physical Science Basis. Contribution of Working Group I to the Sixth Assessment Report of the Intergovernmental Panel on Climate Change, edited by: Masson-Delmotte, V., Zhai, P., Pirani, A., Connors, S. L., Péan, C., Berger, S., Caud, N., Chen, Y., Goldfarb, L., Gomis, M. I., Huang, M., Leitzell, K., Lonnoy, E., Matthews, J. B. R., Maycock, T. K., Waterfield, T., Yelekçi, O., Yu, R., and Zhou, B., Cambridge University Press, Cambridge, United Kingdom, and New York, NY, USA, 923–1054, https://doi.org/10.1017/9781009157896.009, 2021.

Geller, M., Biswas, S., and Sioutas, C.: Determination of Particle Effective Density in Urban Environments with a Differential Mobility Analyzer and Aerosol Particle Mass Analyzer, Aerosol Science and Technology, 40, 709–723, https://doi.org/10.1080/02786820600803925, 2006.

Hadley, O. L. and Kirchstetter, T. W.: Black-carbon reduction of snow albedo, Nature Clim Change, 2, 437–440, https://doi.org/10.1038/nclimate1433, 2012.

Hagler, G. S. W., Bergin, M. H., Smith, E. A., Dibb, J. E., Anderson, C., and Steig, E. J.: Particulate and water-soluble carbon measured in recent snow at Summit, Greenland, Geophysical Research Letters, 34, https://doi.org/10.1029/2007GL030110, 2007.

Hansen, J., Sato, M., Ruedy, R., Nazarenko, L., Lacis, A., Schmidt, G. A., Russell, G., Aleinov, I., Bauer, M., Bauer, S., Bell, N., Cairns, B., Canuto, V., Chandler, M., Cheng, Y., Del Genio, A., Faluvegi, G., Fleming, E., Friend, A., Hall, T., Jackman, C., Kelley, M., Kiang, N., Koch, D., Lean, J., Lerner, J., Lo, K., Menon, S., Miller, R., Minnis, P., Novakov, T., Oinas, V., Perlwitz, Ja., Perlwitz, Ju., Rind, D., Romanou, A., Shindell, D., Stone, P., Sun, S., Tausnev, N., Thresher, D., Wielicki, B., Wong, T., Yao, M., and Zhang, S.: Efficacy of climate forcings, Journal of Geophysical Research: Atmospheres, 110, https://doi.org/10.1029/2005JD005776, 2005.

He, C., Flanner, M. G., Chen, F., Barlage, M., Liou, K.-N., Kang, S., Ming, J., and Qian, Y.: Black carbon-induced snow albedo reduction over the Tibetan Plateau: uncertainties from snow grain shape and aerosol–snow mixing state based on an updated SNICAR model, Atmospheric Chemistry and Physics, 18, 11507–11527, https://doi.org/10.5194/acp-18-11507-2018, 2018.

Hecobian, A., Zhang, X., Zheng, M., Frank, N., Edgerton, E. S., and Weber, R. J.: Water-Soluble Organic Aerosol material and the light-absorption characteristics of aqueous extracts measured over the Southeastern United States, Atmospheric Chemistry and Physics, 10, 5965–5977, https://doi.org/10.5194/acp-10-5965-2010, 2010.

Hems, R. F., Schnitzler, E. G., Liu-Kang, C., Cappa, C. D., and Abbatt, J. P. D.: Aging of Atmospheric Brown Carbon Aerosol, ACS Earth Space Chem., 5, 722–748, https://doi.org/10.1021/acsearthspacechem.0c00346, 2021.

https://doi.org/10.5194/egusphere-2026-6632
Preprint. Discussion started: 19 November 2026
© Author(s) 2026. CC BY 4.0 License.

Hu, Z., Kang, S., Yan, F., Zhang, Y., Li, Y., Chen, P., Qin, X., Wang, K., Gao, S., and Li, C.: Dissolved organic carbon fractionation accelerates glacier-melting: A case study in the northern Tibetan Plateau, Science of The Total Environment, 627, 579–585, https://doi.org/10.1016/j.scitotenv.2018.01.265, 2018.

Huang, R.-J., Yang, L., Shen, J., Yuan, W., Gong, Y., Guo, J., Cao, W., Duan, J., Ni, H., Zhu, C., Dai, W., Li, Y., Chen, Y., Chen, Q., Wu, Y., Zhang, R., Dusek, U., O'Dowd, C., and Hoffmann, T.: Water-Insoluble Organics Dominate Brown Carbon in Wintertime Urban Aerosol of China: Chemical Characteristics and Optical Properties, Environ. Sci. Technol., 54, 7836–7847, https://doi.org/10.1021/acs.est.0c01149, 2020.

Jennings, S. G., Pinnick, R. G., and Gillespie, J. B.: Relation between absorption coefficient and imaginary index of atmospheric aerosol constituents, Appl. Opt., AO, 18, 1368–1371, https://doi.org/10.1364/AO.18.001368, 1979.

Kang, S., Zhang, Y., Chen, P., Guo, J., Zhang, Q., Cong, Z., Kaspari, S., Tripathee, L., Gao, T., Niu, H., Zhong, X., Chen, X., Hu, Z., Li, X., Li, Y., Neupane, B., Yan, F., Rupakheti, D., Gul, C., Zhang, W., Wu, G., Yang, L., Wang, Z., and Li, C.: Black carbon and organic carbon dataset over the Third Pole, Earth System Science Data, 14, 683–707, https://doi.org/10.5194/essd-14-683-2022, 2022.

Kirillova, E. N., Andersson, A., Han, J., Lee, M., and Gustafsson, Ö.: Sources and light absorption of water-soluble organic carbon aerosols in the outflow from northern China, Atmospheric Chemistry and Physics, 14, 1413–1422, https://doi.org/10.5194/acp-14-1413-2014, 2014.

Laskin, A., Laskin, J., and Nizkorodov, S. A.: Chemistry of Atmospheric Brown Carbon, Chem. Rev., 115, 4335–4382, https://doi.org/10.1021/cr5006167, 2015.

Lazarcik, J., Dibb, J. E., Adolph, A. C., Amante, J. M., Wake, C. P., Scheuer, E., Mineau, M. M., and Albert, M. R.: Major fraction of black carbon is flushed from the melting New Hampshire snowpack nearly as quickly as soluble impurities, Journal of Geophysical Research: Atmospheres, 122, 537–553, https://doi.org/10.1002/2016JD025351, 2017.

Li, C., He, Q., Hettiyadura, A. P. S., Käfer, U., Shmul, G., Meidan, D., Zimmermann, R., Brown, S. S., George, C., Laskin, A., and Rudich, Y.: Formation of Secondary Brown Carbon in Biomass Burning Aerosol Proxies through NO3 Radical Reactions, Environ. Sci. Technol., 54, 1395–1405, https://doi.org/10.1021/acs.est.9b05641, 2020.

Liu, D., Taylor, J. W., Young, D. E., Flynn, M. J., Coe, H., and Allan, J. D.: The effect of complex black carbon microphysics on the determination of the optical properties of brown carbon, Geophysical Research Letters, 42, 613–619, https://doi.org/10.1002/2014GL062443, 2015.

Liu, J., Bergin, M., Guo, H., King, L., Kotra, N., Edgerton, E., and Weber, R. J.: Size-resolved measurements of brown carbon in water and methanol extracts and estimates of their contribution to ambient fine-particle light absorption, Atmos. Chem. Phys., 13, 12389–12404, https://doi.org/10.5194/acp-13-12389-2013, 2013.

McMeeking, G. R., Kreidenweis, S. M., Baker, S., Carrico, C. M., Chow, J. C., Collett Jr., J. L., Hao, W. M., Holden, A. S., Kirchstetter, T. W., Malm, W. C., Moosmüller, H., Sullivan, A. P., and Wold, C. E.: Emissions of trace gases and aerosols during the open combustion of biomass in the laboratory, Journal of Geophysical Research: Atmospheres, 114, https://doi.org/10.1029/2009JD011836, 2009.

Meinander, O., Kontu, A., Virkkula, A., Arola, A., Backman, L., Dagsson-Waldhauserová, P., Järvinen, O., Manninen, T., Svensson, J., de Leeuw, G., and Leppäranta, M.: Brief communication: Light-absorbing impurities can reduce the density of melting snow, The Cryosphere, 8, 991–995, https://doi.org/10.5194/tc-8-991-2014, 2014.

https://doi.org/10.5194/egusphere-2026-6632
Preprint. Discussion started: 19 November 2026
© Author(s) 2026. CC BY 4.0 License.

Moosmüller, H., Chakrabarty, R. K., and Arnott, W. P.: Aerosol light absorption and its measurement: A review, Journal of Quantitative Spectroscopy and Radiative Transfer, 110, 844–878, https://doi.org/10.1016/j.jqsrt.2009.02.035, 2009.

Moosmüller, H., Chakrabarty, R. K., Ehlers, K. M., and Arnott, W. P.: Absorption Ångström coefficient, brown carbon, and aerosols: basic concepts, bulk matter, and spherical particles, Atmospheric Chemistry and Physics, 11, 1217–1225, https://doi.org/10.5194/acp-11-1217-2011, 2011.

Mukherjee, A., Hartikainen, A., Somero, M., Luostari, V., Ihalainen, M., Rüger, C. P., Kekäläinen, T., Nissinen, V. H., Barreira, L. M. F., Koponen, H., Kokkola, T., Li, D., Vettikkat, L., Yli-Pirilä, P., Shahzaib, M., Ruppel, M. M., Vakkari, V., Jaars, K., Siebert, S. J., Buchholz, A., Köster, K., van Zyl, P. G., Timonen, H., Kinnunen, N., Jänis, J., Virtanen, A., Virkkula, A., and Sippula, O.: Brown carbon emissions from laboratory combustion of Eurasian arctic-boreal and South African savanna biomass, Atmospheric Chemistry and Physics, 25, 16747–16774, https://doi.org/10.5194/acp-25-16747-2025, 2025.

Norvapalo, O. S. H.: Nokihiukkasten kokojakauman ja morfologian määritys lumessa, Size distribution and morphology of soot particles on snow, M.Sc. thesis, Department of Environmental and Biological Sciences, University of Eastern Finland, 79 pp., https://erepo.uef.fi/items/62e9d14e-0203-4096-91f0-c42d28b05f15, 2024 (in Finnish)

Peltoniemi, J. I., Gritsevich, M., Hakala, T., Dagsson-Waldhauserová, P., Arnalds, Ó., Anttila, K., Hannula, H.-R., Kivekäs, N., Lihavainen, H., Meinander, O., Svensson, J., Virkkula, A., and de Leeuw, G.: Soot on Snow experiment: bidirectional reflectance factor measurements of contaminated snow, The Cryosphere, 9, 2323–2337, https://doi.org/10.5194/tc-9-2323-2015, 2015.

Petzold, A., Ogren, J. A., Fiebig, M., Laj, P., Li, S.-M., Baltensperger, U., Holzer-Popp, T., Kinne, S., Pappalardo, G., Sugimoto, N., Wehrli, C., Wiedensohler, A., and Zhang, X.-Y.: Recommendations for reporting "black carbon" measurements, Atmospheric Chemistry and Physics, 13, 8365–8379, https://doi.org/10.5194/acp-13-8365-2013, 2013.

Phillips, S. M. and Smith, G. D.: Spectroscopic comparison of water- and methanol-soluble brown carbon particulate matter, Aerosol Science and Technology, 51, 1113–1121, https://doi.org/10.1080/02786826.2017.1334109, 2017.

Rantanen, M., Karpechko, A. Y., Lipponen, A., Nordling, K., Hyvärinen, O., Ruosteenoja, K., Vihma, T., and Laaksonen, A.: The Arctic has warmed nearly four times faster than the globe since 1979, Commun Earth Environ, 3, 1–10, https://doi.org/10.1038/s43247-022-00498-3, 2022.

Ruppel, Meri. M., Somero, M., Sippula, O., Ihalainen, M., Louhisalmi, J., Tissari, J., Haghipour, N., Ström, J., Väliranta, M., Köster, K., Vakkari, V., Jaars, K., Huang, L., and Smittenberg, R. H.: Arctic and Boreal Wildfires Impact Climate by Releasing Ancient Carbon and Light-Absorbing Particles, Environ. Sci. Technol., 60, 11608–11620, https://doi.org/10.1021/acs.est.5c17130, 2026.

Saleh, R.: From Measurements to Models: Toward Accurate Representation of Brown Carbon in Climate Calculations, Curr Pollution Rep, 6, 90–104, https://doi.org/10.1007/s40726-020-00139-3, 2020.

Saleh, R., Robinson, E. S., Tkacik, D. S., Ahern, A. T., Liu, S., Aiken, A. C., Sullivan, R. C., Presto, A. A., Dubey, M. K., Yokelson, R. J., Donahue, N. M., and Robinson, A. L.: Brownness of organics in aerosols from biomass burning linked to their black carbon content, Nature Geosci, 7, 647–650, https://doi.org/10.1038/ngeo2220, 2014.

Shamjad, P. M., Satish, R. V., Thamban, N. M., Rastogi, N., and Tripathi, S. N.: Absorbing Refractive Index and Direct Radiative Forcing of Atmospheric Brown Carbon over Gangetic Plain, ACS Earth Space Chem., 2, 31–37, https://doi.org/10.1021/acsearthspacechem.7b00074, 2018.

https://doi.org/10.5194/egusphere-2026-6632
Preprint. Discussion started: 19 November 2026
© Author(s) 2026. CC BY 4.0 License.

Shen, Z., Lei, Y., Zhang, L., Zhang, Q., Zeng, Y., Tao, J., Zhu, C., Cao, J., Xu, H., and Liu, S.: Methanol Extracted Brown Carbon in PM2.5 Over Xi'an, China: Seasonal Variation of Optical Properties and Sources Identification, Aerosol Sci Eng, 1, 57–65, https://doi.org/10.1007/s41810-017-0007-z, 2017.

Simoneit, B. R. T.: Biomass burning — a review of organic tracers for smoke from incomplete combustion, Applied Geochemistry, 17, 129–162, https://doi.org/10.1016/S0883-2927(01)00061-0, 2002.

Sterle, K. M., McConnell, J. R., Dozier, J., Edwards, R., and Flanner, M. G.: Retention and radiative forcing of black carbon in eastern Sierra Nevada snow, The Cryosphere, 7, 365–374, https://doi.org/10.5194/tc-7-365-2013, 2013.

Sumlin, B. J., Heinson, Y. W., Shetty, N., Pandey, A., Pattison, R. S., Baker, S., Hao, W. M., and Chakrabarty, R. K.: UV–Vis–IR spectral complex refractive indices and optical properties of brown carbon aerosol from biomass burning, Journal of Quantitative Spectroscopy and Radiative Transfer, 206, 392–398, https://doi.org/10.1016/j.jqsrt.2017.12.009, 2018.

Svensson, J., Leppänen, L., Hannula, H.-R., Kontu, A., Shen, Y., Meinander, O., Dagsson-Waldhauserová, P., Mesceriakovas, A., Heikkinen, E., Ruppel, M., Sippula, O., Ström, J., Asmi, E., and Virkkula, A.: Soot-on-snow experiment: artificial deposition of light-absorbing particles onto snow surfaces in 2018, Front. Earth Sci., 12, https://doi.org/10.3389/feart.2024.1358155, 2024.

Voisin, D., Jaffrezo, J.-L., Houdier, S., Barret, M., Cozic, J., King, M. D., France, J. L., Reay, H. J., Grannas, A., Kos, G., Ariya, P. A., Beine, H. J., and Domine, F.: Carbonaceous species and humic like substances (HULIS) in Arctic snowpack during OASIS field campaign in Barrow, Journal of Geophysical Research: Atmospheres, 117, https://doi.org/10.1029/2011JD016612, 2012.

Wang, X., Doherty, S. J., and Huang, J.: Black carbon and other light-absorbing impurities in snow across Northern China, Journal of Geophysical Research: Atmospheres, 118, 1471–1492, https://doi.org/10.1029/2012JD018291, 2013.

Xu, B.-Q., Wang, M., Joswiak, D. R., Cao, J.-J., Yao, T.-D., Wu, G.-J., Yang, W., and Zhao, H.-B.: Deposition of anthropogenic aerosols in a southeastern Tibetan glacier, Journal of Geophysical Research: Atmospheres, 114, https://doi.org/10.1029/2008JD011510, 2009.

Yan, F., Kang, S., Li, C., Zhang, Y., Qin, X., Li, Y., Zhang, X., Hu, Z., Chen, P., Li, X., Qu, B., and Sillanpää, M.: Concentration, sources and light absorption characteristics of dissolved organic carbon on a medium-sized valley glacier, northern Tibetan Plateau, The Cryosphere, 10, 2611–2621, https://doi.org/10.5194/tc-10-2611-2016, 2016.

Yan, F., Kang, S., Sillanpää, M., Hu, Z., Gao, S., Chen, P., Gautam, S., Reinikainen, S.-P., and Li, C.: A new method for extraction of methanol-soluble brown carbon: Implications for investigation of its light absorption ability, Environmental Pollution, 262, 114300, https://doi.org/10.1016/j.envpol.2020.114300, 2020.

Zhang, Y., Kang, S., Gao, T., Schmale, J., Liu, Y., Zhang, W., Guo, J., Du, W., Hu, Z., Cui, X., and Sillanpää, M.: Dissolved organic carbon in snow cover of the Chinese Altai Mountains, Central Asia: Concentrations, sources and light-absorption properties, Science of The Total Environment, 647, 1385–1397, https://doi.org/10.1016/j.scitotenv.2018.07.417, 2019.

Zhu, C.-S., Cao, J.-J., Huang, R.-J., Shen, Z.-X., Wang, Q.-Y., and Zhang, N.-N.: Light absorption properties of brown carbon over the southeastern Tibetan Plateau, Science of The Total Environment, 625, 246–251, https://doi.org/10.1016/j.scitotenv.2017.12.183, 2018.

Zhu, C.-S., Qu, Y., Huang, H., Shi, J.-L., Dai, W.-T., Zhang, N.-N., Wang, N., Wang, L.-Y., Ji, S.-S., and Cao, J.-J.: Brown Carbon From Biomass Burning Reinforces the Himalayas and Tibetan Plateau Warming, Geophysical Research Letters, 51, e2023GL107269, https://doi.org/10.1029/2023GL107269, 2024.